15

Cyclotrons and Synchrotrons

The term *circular accelerator* refers to any machine in which beams describe a closed orbit. All circular accelerators have a vertical magnetic field to bend particle trajectories and one or more gaps coupled to inductively isolated cavities to accelerate particles. Beam orbits are often not true circles; for instance, large synchrotrons are composed of alternating straight and circular sections. The main characteristic of resonant circular accelerators is synchronization between oscillating acceleration fields and the revolution frequency of particles.

Particle recirculation is a major advantage of resonant circular accelerators over rf linacs. In a circular machine, particles pass through the same acceleration gap many times (10^2 to greater than 10^8). High kinetic energy can be achieved with relatively low gap voltage. One criterion to compare circular and linear accelerators for high-energy applications is the energy gain per length of the machine; the cost of many accelerator components is linearly proportional to the length of the beamline. Dividing the energy of a beam from a conventional synchrotron by the circumference of the machine gives effective gradients exceeding 50 MV/m. The gradient is considerably higher for accelerators with superconducting magnets. This figure of merit has not been approached in either conventional or collective linear accelerators.

There are numerous types of resonant circular accelerators, some with specific advantages and some of mainly historic significance. Before beginning a detailed study, it is useful to review briefly existing classes of accelerators. In the following outline, a standard terminology is defined and the significance of each device is emphasized.

Cyclotrons and Synchrotrons

Most resonant circular accelerators can be classed as either cyclotrons or synchrotrons. One exception is the microtron (Section 14.7), which is technologically akin to linear accelerators. The microtron may be classified as a cyclotron for relativistic electrons, operating well beyond the transition energy (see Section 15.6). The other exception is the synchrocyclotron (Section 15.4).

A. Cyclotron

A cyclotron has constant magnetic field magnitude and constant rf frequency. Beam energy is limited by relativistic effects, which destroy synchronization between particle orbits and rf fields. Therefore, the cyclotron is useful only for ion acceleration. The virtue of cyclotrons is that they generate a continuous train of beam micropulses. Cyclotrons are characterized by large-area magnetic fields to confine ions from zero energy to the output energy.

1. Uniform-Field Cyclotron

The uniform-field cyclotron has considerable historic significance. It was the first accelerator to generate multi-MeV particle beams for nuclear physics research. The vertical field is uniform in azimuth. The field magnitude is almost constant in the radial direction, with small positive field index for vertical focusing. Resonant acceleration in the uniform-field cyclotron depends on the constancy of the non-relativistic gyrofrequency. The energy limit for light ion beams is about 15-20 MeV, determined by relativistic mass increase and the decrease of magnetic field with radius. There is no synchronous phase in a uniform-field cyclotron.

2. Azimuthally-Varying-Field (AVF) Cyclotron

The AVF cyclotron is a major improvement over the uniform-field cyclotron. Variations are added to the confining magnetic field by attaching wedge-shaped inserts at periodic azimuthal positions of the magnet poles. The extra horizontal-field components enhance vertical focusing. It is possible to tolerate an average negative-field index so that the bending field increases with radius. With proper choice of focusing elements and field index variation, the magnetic field variation balances the relativistic mass increase, resulting in a constant-revolution frequency. An AVF cyclotron with this property is called an isochronous cyclotron. An additional advantage of AVF cyclotrons is that the stronger vertical focusing allows higher beam intensity. AVF machines have supplanted the uniform-field cyclotron, even in low-energy applications.

3. Separated-Sector Cyclotron

The separated-sector cyclotron is a special case of the AVF cyclotron. The azimuthal field variation results from splitting the bending magnet into a number of sectors. The advantages of the separated sector cyclotron are (1) modular magnet construction and (2) the ability to locate rf feeds and acceleration gaps between the sectors. The design of separated-sector cyclotrons is complicated by the fact that particles cannot be accelerated from low energy. This feature can be used to advantage; beams with lower emittance (better coherence) are achieved if an independent accelerator is used for low-energy acceleration.

4. Spiral Cyclotron

The pole inserts in a spiral cyclotron have spiral boundaries. Spiral shaping is used in both standard AVF and separated-sector machines. In a spiral cyclotron, ion orbits have an inclination at the boundaries of high-field regions. Vertical confinement is enhanced by edge focusing (Section 6.9). The combined effects of edge focusing and defocusing lead to an additional vertical confinement force.

5. Superconducting Cyclotron

Superconducting cyclotrons have shaped iron magnet poles that utilize the focusing techniques outlined above. The magnetizing force is supplied by superconducting coils, which consume little power. Superconducting cyclotrons are typically compact machines because they are operated at high fields, well above the saturation level of the iron poles. In this situation, all the magnetic dipoles in the poles are aligned; the net fields can be predicted accurately.

B. Synchrocyclotron

The synchrocyclotron is a precursor of the synchrotron. It represents an early effort to extend the kinetic energy limits of cyclotrons. Synchrocyclotrons have a constant magnetic field with geometry similar to the uniform-field cyclotron. The main difference is that the rf frequency is varied to maintain particle synchronization into the relativistic regime. Synchrocyclotrons are cyclic machines with a greatly reduced time-averaged output flux compared to a cyclotron. Kinetic energies for protons to 1 GeV have been achieved. In the sub-GeV energy range, synchrocyclotrons were supplanted by AVF cyclotrons, which generate a continuous beam. Synchrocyclotrons have not been extended to higher energy because of technological and economic difficulties in fabricating the huge, monolithic magnets that characterize the machine.

C. Synchrotron

Synchrotrons are the present standard accelerators for particle physics research. They are cycled machines. Both the magnitude of the magnetic field and the rf frequency are varied to maintain a synchronous particle at a constant orbit radius. The constant-radius feature is very important; bending and focusing fields need extend over only a small ring-shaped volume. This minimizes the cost of the magnets, allowing construction of large-diameter machines for ion energies of up to 800 GeV. Synchrotrons are used to accelerate both ions and electrons, although electron machines are limited in energy by emission of synchrotron radiation. The main limits on achievable energy for ions are the cost of the machine and availability of real estate. Cycling times are long in the largest machines, typically many seconds. Electron synchrotrons and proton boosters cycle at frequencies in the range of 15 to 60 Hz.

1. Weak Focusing Synchrotron

Early synchrotrons used weak focusing. The bending magnets were shaped to produce a field with index in the range $0 < n < 1$. With low focusing force, the combined effects of transverse particle velocity and synchrotron oscillations (see Section 15.6) resulted in beams with large cross section. This implies costly, large-bore magnets.

2. Strong Focusing Synchrotron

All modern synchrotrons use transverse focusing systems composed of strong lenses in a focusing-defocusing array. Strong focusing minimizes the beam cross section, reducing the magnet size. Beam dynamics are more complex in a strong focusing synchrotron. The magnets must be constructed and aligned with high precision, and care must be taken to avoid resonance instabilities. Advances in magnet technology and beam theory have made it possible to overcome these difficulties.

Alternating Gradient Synchrotron (AGS). The bending field in an alternating gradient synchrotron is produced by a ring of wedge-shaped magnets which fit together to form an annular region of vertical field. The magnets have alternate positive and negative field gradient with n » 1. The combination of focusing and defocusing in the horizontal and vertical directions leads to net beam confinement.

Separated Function Synchrotron. Most modern synchrotrons are configured as separated function synchrotrons. The bending field is provided by sector magnets with uniform vertical field. Focusing is performed by quadrupole magnetic lens set between the bending magnets. Other magnets may be included for correction of beam optics.

3. Storage Ring

A storage ring usually has the same focusing and bending field configuration as a separated function synchrotron, but provides no acceleration. The magnetic fields are constant in time. An rf cavity may be included for longitudinal beam manipulations such as stacking or, in the case of electrons, maintaining kinetic energy in the presence of radiation loss. A storage ring contains energetic particles at constant energy for long periods of time. The primary applications are for colliding beam experiments and synchrotron radiation production.

4. Collider

A collider is a synchrotron, storage ring, dual synchrotron, or dual storage ring with special geometry to allow high-energy charged particles moving in opposite directions to collide head-on at a number of positions in the machine. The use of colliding beams significantly increases the amount of energy available to probe the structure of matter for elementary particle physics. Colliders have been operated (or are planned) for counter-rotating beams of protons (*pp* collider), electrons and positrons (e^-e^+), and protons and antiprotons ($p\bar{p}$).

Section 15.1 introduces the uniform-field cyclotron and the principles of circular resonant accelerators. The longitudinal dynamics of the uniform-field cyclotron is reviewed in Section 15.2. The calculations deal with an interesting application of the phase equations when there is no synchronous particle. The model leads to the choice of optimum acceleration history and to limits on achievable kinetic energy. Sections 15.3 and 15.4 are concerned with AVF, or isochronous, cyclotrons. Transverse focusing is treated in the first section. Section 15.4 summarizes relationships between magnetic field and rf frequency to preserve synchronization in fixed-field, fixed-frequency machines. There is also a description of the synchrocyclotron.

Sections 15.5-15.7 are devoted to the synchrotron. The first section describes general features of synchrotrons, including focusing systems, energy limits, synchrotron radiation, and the kinematics of colliding beams. The longitudinal dynamics of synchrotrons is the subject of Section 15.6. Material includes constraints on magnetic field and rf frequency variation for synchronization, synchrotron oscillations, and the transition energy. To conclude, Section 15.7 summarizes the principles and benefits of strong focusing. Derivations are given to illustrate the effects of alignment errors in a strong focusing system. Forbidden numbers of betatron wavelengths and mode coupling are discussed qualitatively.

15.1 PRINCIPLES OF THE UNIFORM-FIELD CYCLOTRON

The operation of the uniform-field cyclotron [E. 0. Lawrence, Science **72**, 376 (1930)] is based on the fact that the gyrofrequency for non-relativistic ions [Eq. (3.39)] is independent of kinetic energy. Resonance between the orbital motion and an accelerating electric field can be achieved for ion kinetic energy that is small compared to the rest energy. The configuration of the uniform-field cyclotron is illustrated in Figure 15.1a. Ions are constrained to circular orbits by a

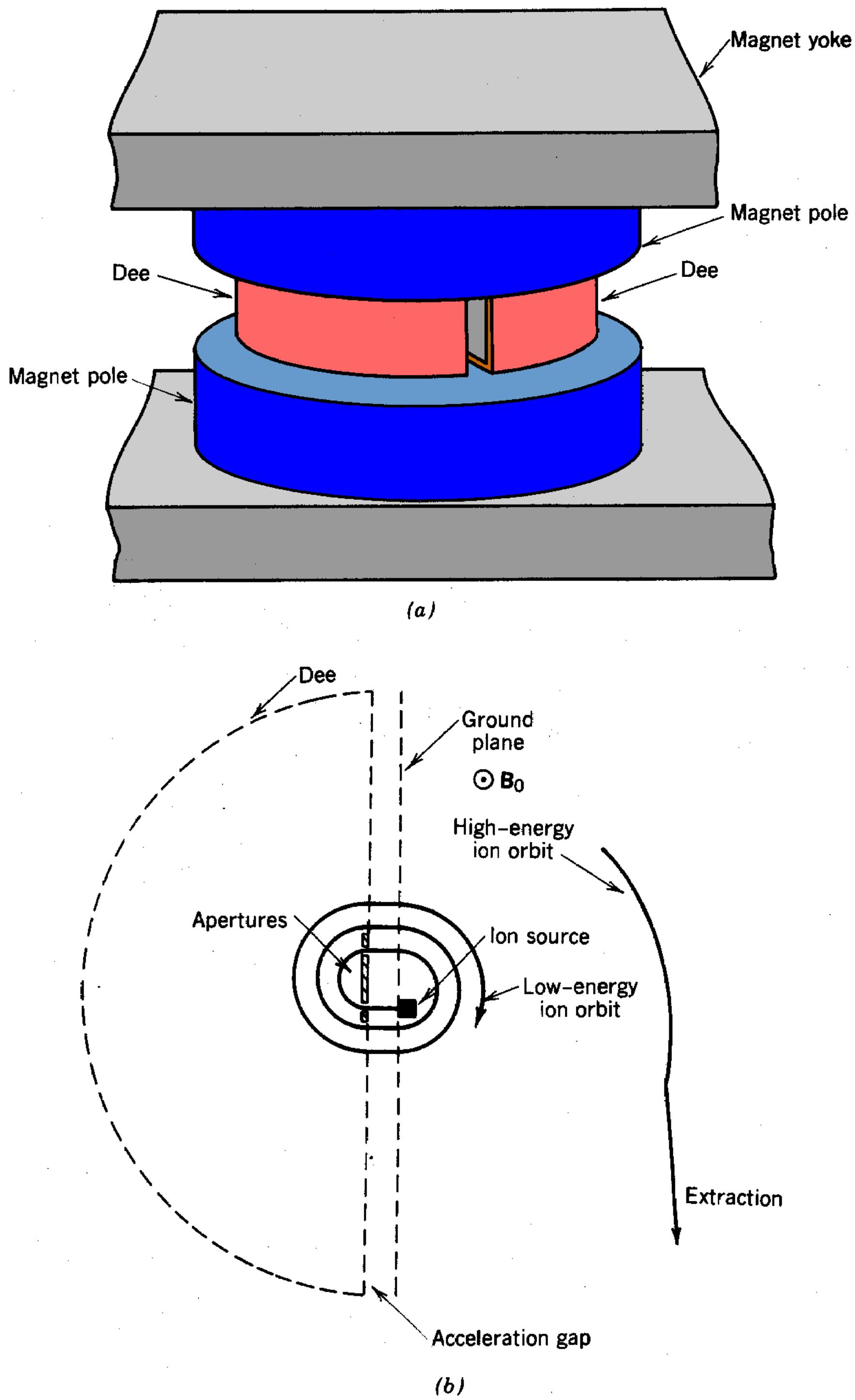

Figure 15.1 Uniform-field cyclotron. (*a*) General layout of beam acceleration region. (*b*) Overhead sectional view of acceleration region, showing a cyclotron with one dee and a ground plane. A single dee facilitates injection and extraction.

vertical field between the poles of a magnet. The ions are accelerated in the gap between two D-shaped metal structures (dees) located within the field region. An ac voltage is applied to the dees by an rf resonator. The resonator is tuned to oscillate near ω_g.

The acceleration history of an ion is indicated in Figure 15.1b. The accelerator illustrated has only one dee excited by a bipolar waveform to facilitate extraction. A source, located at the center of the machine continuously generates ions. The low-energy ions are accelerated to the opposite electrode during the positive-polarity half of the rf cycle. After crossing the gap, the ions are shielded from electric fields so that they follow a circular orbit. When the ions return to the gap after a time interval π/ω_{go} they are again accelerated because the polarity of the dee voltage is reversed. An aperture located at the entrance to the acceleration gap limits ions to a small range of phase with respect to the rf field. If the ions were not limited to a small phase range, the output beam would have an unacceptably large energy spread. In subsequent gap crossings, the ion kinetic energy and gyroradius increase until the ions are extracted at the periphery of the magnet. The cyclotron is similar to the Wideröe linear accelerator (Section 14.2); the increase in the gyroradius with energy is analogous to the increase in drift-tube length for the linear machine.

The rf frequency in cyclotrons is relatively low. The ion gyrofrequency is

$$f_o = qB_o/2\pi m_i = (1.52\times 10^7)\ B_o(tesla)/A, \tag{15.1}$$

where A is the atomic mass number, m_i/m_p. Generally, frequency is in the range of 10 MHz for magnetic fields near 1 T. The maximum energy of ions in a cyclotron is limited by relativistic detuning and radial variations of the magnetic field magnitude. In a uniform-field magnet field, the kinetic energy and orbit radius of non-relativistic ions are related by

$$T_{\max} = 48\ (Z^*RB)^2/A, \tag{15.2}$$

where $T_{\max}$ is given in MeV, R in meters, and B in tesla. For example, 30-MeV deuterons require a 1-T field with good uniformity over a 1.25-m radius.

Transverse focusing in the uniform-field cyclotron is performed by an azimuthally symmetric vertical field with a radial gradient (Section 7.3). The main differences from the betatron are that the field index is small compared to unity ($\nu_r \cong 1$ and $\nu_z \ll 1$) and that particle orbits extend over a wide range of radii. Figure 15.2 diagrams magnetic field in a typical uniform-field cyclotron magnet and indicates the radial variation of field magnitude and field index, n. The field index is not constant with radius. Symmetry requires that the field index be zero at the center of the magnet. It increases rapidly with radius at the edge of the pole. Cyclotron magnets are designed for small n over most of the field area to minimize desynchronization of particle orbits. Therefore, vertical focusing in a uniform-field cyclotron is weak.

There is no vertical magnetic focusing at the center of the magnet. By a fortunate coincidence,

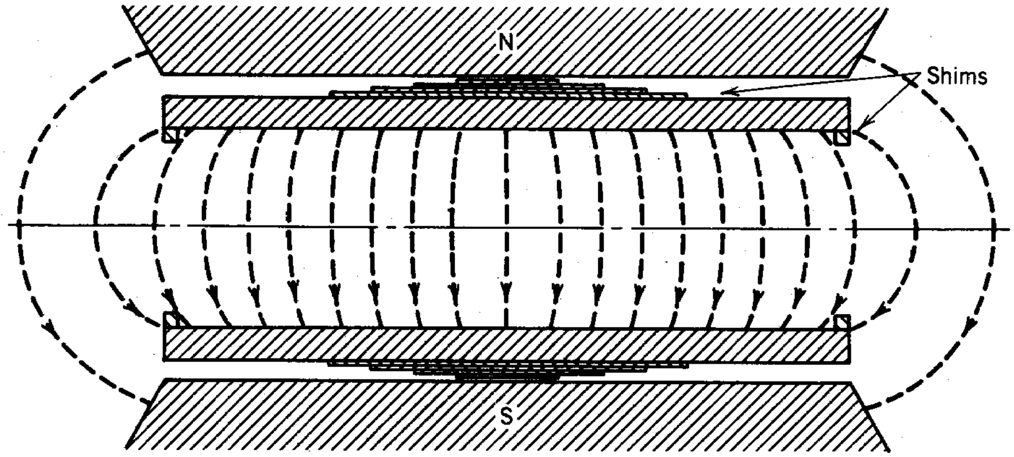

(a)

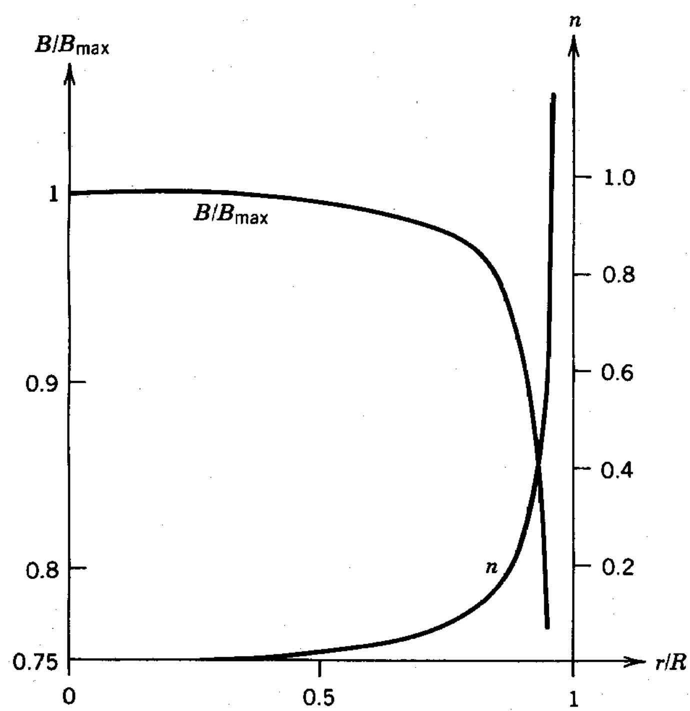

(b)

Figure 15.2 Magnetic fields of uniform-field cyclotron. (*a*) Sectional view of cyclotron magnetic poles showing shims for optimizing field distribution. (*b*) Radial variation of vertical field magnitude and field index. (M. S. Livingston and J. P. Blewett, *Particle Accelerators*, used by permission, McGraw-Hill Book Co.)

electrostatic focusing by the accelerating fields is effective for low-energy ions. The electric field pattern between the dees of a cyclotron act as the one-dimensional equivalent of the electrostatic immersion lens discussed in Section 6.6. The main difference from the electrostatic lens is that ion transit-time effects can enhance or reduce focusing. For example, consider the portion of the accelerating half-cycle when the electric field is rising. Ions are focused at the entrance side of the gap and defocused at the exit. When the transit time is comparable to the rf half-period, the transverse electric field is stronger when the ions are near the exit, thereby reducing the net focusing. The converse holds in the part of the accelerating half-cycle with falling field.

In order to extract ions from the machine at a specific location, deflection fields must be applied. Deflection fields should affect only the maximum energy ions. Ordinarily, static electric (magnetic) fields in vacuum extend a distance comparable to the spacing between electrodes (poles) by the properties of the Laplace equation (Section 4.1). Shielding of other ions is accomplished with a septum (separator), an electrode or pole that carries image charge or current to localize deflection fields. An electrostatic septum is illustrated in Figure 15.3. A strong radial electric field deflects maximum energy ions to a radius where $n > 1$. Ions spiral out of the machine

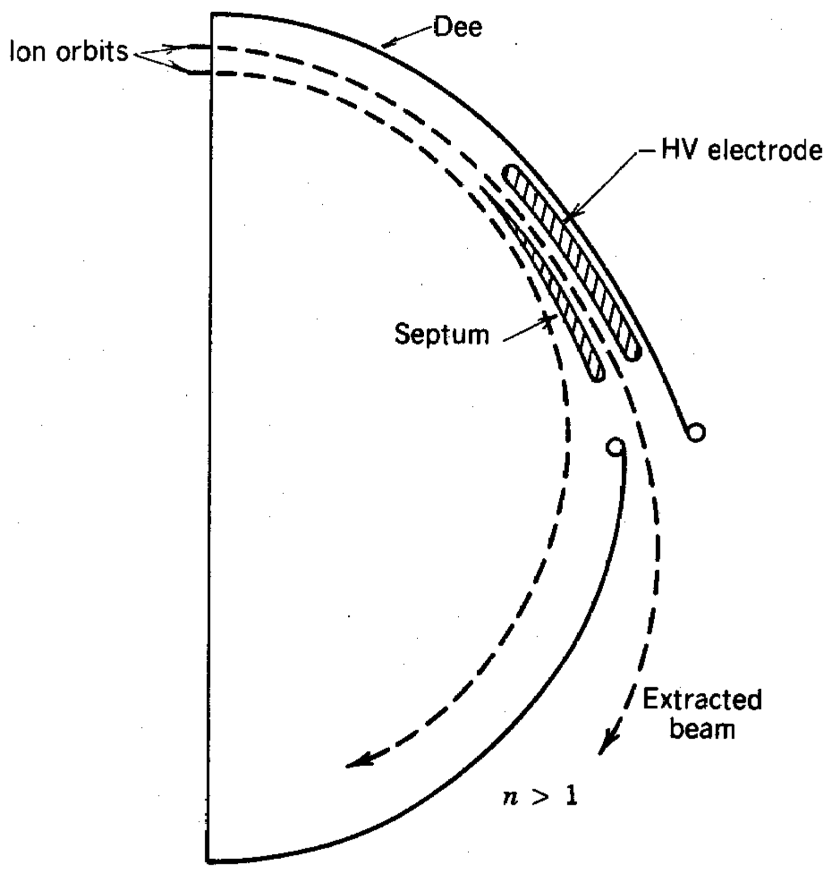

Figure 15.3 Extraction of high-energy ions from cyclotron using electrostatic septum.

along a well-defined trajectory. Clearly, a septum should not intercept a substantial fraction of the beam. Septa are useful in the cyclotron because there is a relatively large separation between orbits. The separation for non-relativistic ions is

$$\Delta R \cong (R/2)\ (2qV_o \sin\varphi_s/T). \tag{15.3}$$

For example, with a peak dee voltage V_o = 100 kV, φ_s = 60°, R = 1 m, and T = 20 MeV, Eq. (15.3) implies that ΔR = 0.44 cm.

15.2 LONGITUDINAL DYNAMICS OF THE UNIFORM-FIELD CYCLOTRON

In the uniform-field cyclotron, the oscillation frequency of gap voltage remains constant while the ion gyrofrequency continually decreases. The reduction in ω_g with energy arises from two causes: (1) the relativistic increase in ion mass and (2) the reduction of magnetic field magnitude at large radius. Models of longitudinal particle motion in a uniform-field cyclotron are similar to those for a traveling wave linear electron accelerator (Section 13.6); there is no synchronous phase. In this section, we shall develop equations to describe the phase history of ions in a uniform-field cyclotron. As in the electron linac, the behavior of a pulse of ions is found by following individual orbits rather than performing an orbit expansion about a synchronous particle. The model predicts the maximum attainable energy and energy spread as a function of the phase width of the ion pulse. The latter quantity is determined by the geometry of the aperture illustrated in Figure 15.1. The model indicates strategies to maximize beam energy.

The geometry of the calculation is illustrated in Figure 15.4. Assume that the voltage of dee1 relative to dee2 is given by

$$V(t) = V_o \sin\omega t, \tag{15.4}$$

where ω is the rf frequency. The following simplifying assumptions facilitate development of a phase equation:

1. Effects of the gap width are neglected. This is true when the gap width divided by the ion velocity is small compared to $1/\omega$.

2. The magnetic field is radially uniform. The model is easily extended to include the effects of field variations.

3. The ions circulate many times during the acceleraton cycle, so that it is sufficient to approximate kinetic energy as a continuous variable and to identify the centroid of the particle orbits with the symmetry axis of the machine.

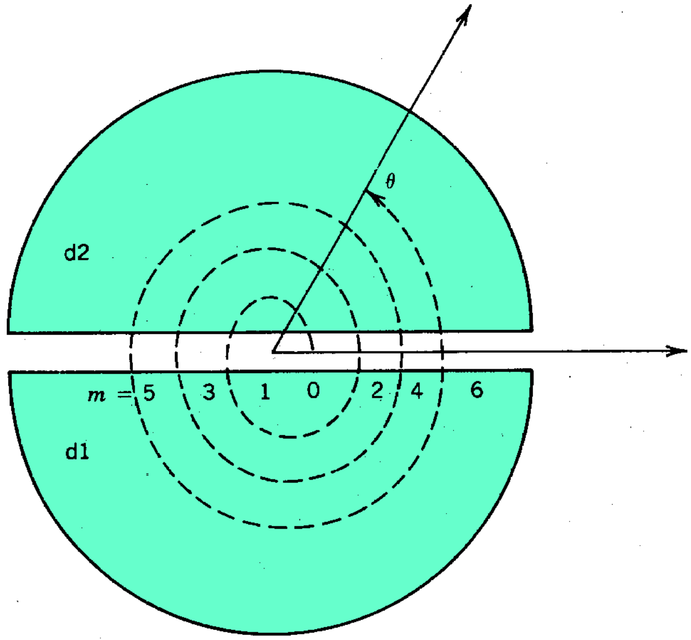

Figure 15.4 Geometry for treating longitudinal dynamics of uniform-field cyclotron.

The phase of an ion at azimuthal position θ and time *t* is defined as

$$\varphi = \omega t - \theta(t). \tag{15.5}$$

Equation (15.5) is consistent with our previous definition of phase (Chapter 13). Particles crossing the gap from deel to dee2 at $t = 0$ have $\varphi = 0$ and experience zero accelerating voltage. The derivative of Eq. (15.5) is

$$d\varphi/dt = \omega - d\theta/dt = \omega - \omega_g, \tag{15.6}$$

where

$$\omega_g = qB_o/\gamma m_i = qc^2B_o/E. \tag{15.7}$$

The quantity E in Eq. (15.7) is the total relativistic ion energy, $E = T + m_ic^2$. In the limit that $T \ll m_ic^2$, the gyrofrequency is almost constant and Eq. (15.6) implies that particles have constant phase during acceleration. Relativistic effects reduce the second term in Eq. (15.6). If the rf frequency equals the non-relativistic gyrofrequency $\omega = \omega_{go}$, then $d\varphi/dt$ is always positive. The limit of acceleration occurs when φ reaches 180°. In this circumstance, ions arrive at the gap when the accelerating voltage is zero; ions are trapped at a particular energy and circulate in the cyclotron at constant radius.

Equation (15.4), combined with the assumption of small gap width, implies that particles making their *m*th transit of the gap with phase φ_m gain an energy.

$$\Delta E_m = qV_o \sin\varphi_m. \tag{15.8}$$

In order to develop an analytic phase equation, it is assumed that energy increases continually and that phase is a continuous function of energy, $\varphi(E)$. The change of phase for a particle during the transit through a dee is

$$\Delta\varphi = (d\varphi/dt)\ (\pi/\omega_g) = \pi\ [(\omega E/c^2 qB_o) - 1]. \tag{15.9}$$

Dividing Eq. (15.9) by Eq. (15.8) gives an approximate equation for $\varphi(E)$:

$$\Delta\varphi/\Delta E \cong d\varphi/dE \cong (\pi/qV_o \sin\varphi)\ [(\omega E/c^2 qB_o) - 1]. \tag{15.10}$$

Equation (15.10) can be rewritten

$$\sin\varphi\ d\varphi = (\pi/qV_o)\ [(\omega E/c^2 qB_o) - 1]\ dE. \tag{15.11}$$

Integration of Eq. (15.11) gives an equation for phase as a function of particle energy:

$$\cos\varphi = \cos\varphi_o - (\pi/qV_o)\ [(\omega/2c^2 qB_o)\ (E^2 - E_o) - (E - E_o)], \tag{15.12}$$

where φ_o is the injection phase. The cyclotron phase equation is usually expressed in terms of the kinetic energy T. Taking $T = E - m_{oc}^2$ and $\omega_{go} = qB_o/m_i$, Eq. (15.12) becomes

$$\cos\varphi = \cos\varphi_o - (\pi/qV_o)\ (1 - \omega/\omega_{go})\ T - (\pi/2qV_o m_i c^2)\ (\omega/\omega_{go})\ T^2. \tag{15.13}$$

During acceleration, ion phase may traverse the range $0° < \varphi < 180°$. The content of Eq. (15.13) can be visualized with the help of Figure 15.5. The quantity $\cos\varphi$ is plotted versus T with φ_o as a parameter. The curves are parabolas. In Figure 15.5a, the magnetic field is adjusted so that $\omega = \omega_o$. The maximum kinetic energy is defined by the intersection of the curve with $\cos\varphi = -1$. The best strategy is to inject the particles in a narrow range near $\varphi_o = 0$. Clearly, higher kinetic energy can be obtained if $\omega < \omega_o$(Fig. 15.5b). The particle is injected with $\varphi_o > 0$. It initially gains on the rf field phase and then lags. A particle phase history is valid only if $\cos\varphi$ remains between -1 and +1. In Figure 15.5b, the orbit with $\varphi_o = 45°$ is not consistent with acceleration to high energy. The curve for $\varphi_o = 90°$ leads to a higher final energy than $\varphi_o = 135°$.

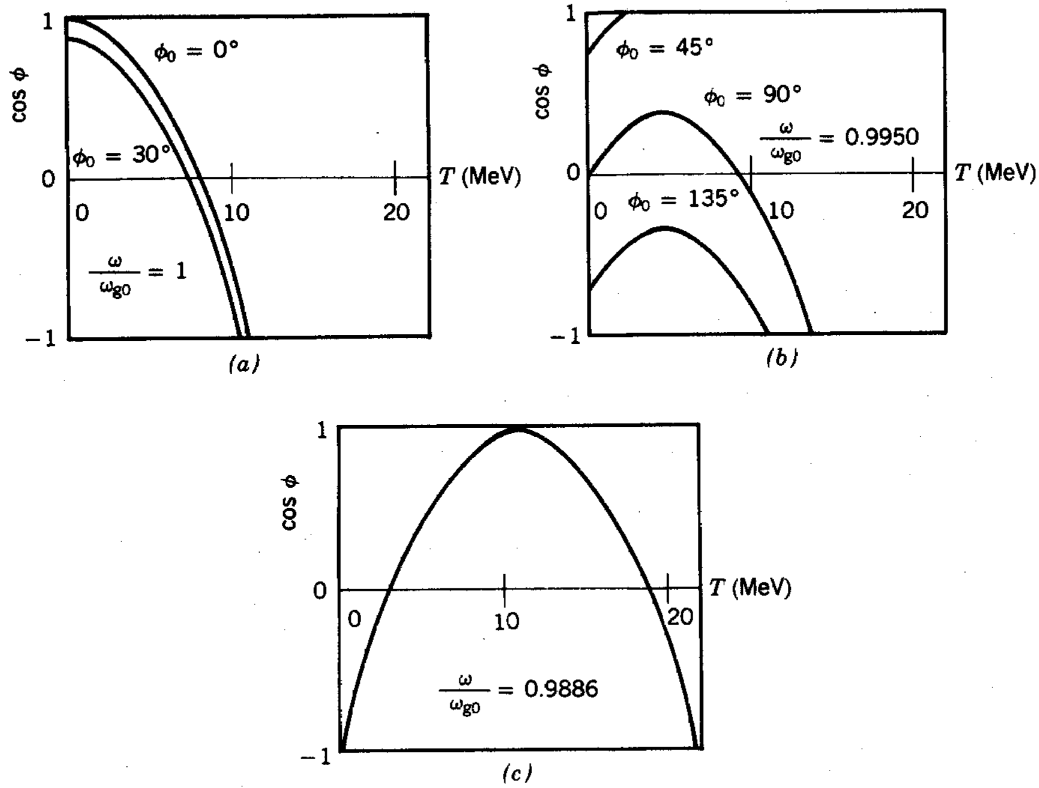

Figure 15.5 Phase histories of protons in uniform-field cyclotron; cos ϕ versus kinetic energy (T) for different injection phase (ϕ_0). (a) $\omega/\omega_{g0} = 1$, where ω is rf angular frequency and ω_{g0} is nonrelativistic gyrofrequency. (b) $\omega/\omega_{g0} = 0.9950$. ($c$) $\omega/\omega_{g0} = 0.9896$, $\phi_0 = 180°$ (parameters for maximum kinetic energy).

The curves of Figure 15.5 depend on V_o, m_i, and ω/ω_{go}. The maximum achievable energy corresponds to the curve illustrated in Figure 15.5c. The particle is injected at $\varphi_o = 180°$. The rf frequency is set lower than the non-relativistic ion gyrofrequency. The two frequencies are equal when φ approaches 0°. The curve of Figure 15.5c represents the maximum possible phase excursion of ions during acceleration and therefore the longest possible time of acceleration. Defining T_{max} as the maximum kinetic energy, Figure 15.5c implies, the constraints

$$\cos\varphi = -1 \quad \textit{for} \quad T = T_{max} \tag{15.14}$$

and

$$\cos\varphi = +1 \quad \textit{for} \quad T = ½T_{max}. \tag{15.15}$$

The last condition proceeds from the symmetric shape of the parabolic curve. Substitution of Eqs. (15.14) and (15.15) in Eq. (15.13) gives two equations in two unknowns for T_{max} and ω/ω_{go}. The solution is

$$\omega/\omega_{go} = 1/(1 + T_{\max}/2m_i c^2) \tag{15.16}$$

and

$$T_{\max} \cong \sqrt{16qV_o m_i c^2/\pi}. \tag{15.17}$$

Equation (15.17) is a good approximation when $T \ll m_i c^2$.

Note that the final kinetic energy is maximized by taking V_o large. This comes about because a high gap voltage accelerates particles in fewer revolutions so that there is less opportunity for particles to get out of synchronization. Typical acceleration gap voltages are ±100 kV. Inspection of Eq. (15.17) indicates that the maximum kinetic energy attainable is quite small compared to $m_i c^2$. In a typical cyclotron, the relativistic mass increase amounts to less than 2%. The small relativistic effects are important because they accumulate over many particle revolutions.

To illustrate typical parameters, consider acceleration of deuterium ions. The rest energy is 1.9 GeV. If V_o = 100 kV, Eq. (15.17) implies that $T_{\max}$ = 31 MeV. The peak energy will be lower if radial variations of magnetic field are included. With B_o = 1.5 T, the non-relativistic gyrofrequency is f_o = 13.6 MHz. For peak kinetic energy, the rf frequency should be about 13.5 MHz. The ions make approximately 500 revolutions during acceleration.

15.3 FOCUSING BY AZIMUTHALLY VARYING FIELDS (AVF)

Inspection of Eqs. (15.6) and (15.7) shows that synchronization in a cyclotron can be preserved only if the average bending magnetic field increases with radius. A positive field gradient corresponds to a negative field index in a magnetic field with azimuthal symmetry, leading to vertical defocusing. A positive field index can be tolerated if there is an extra source of vertical focusing. One way to provide additional focusing is to introduce azimuthal variations in the bending field. In this section, we shall study particle orbits in azimuthally varying fields. The intent is to achieve a physical understanding of AVF focusing through simple models. The actual design of accelerators with AVF focusing [K.R. Symon, *et. al.*, Phys. Rev. **103**, 1837 (1956); F.T. Cole, *et .al.*, Rev. Sci. Instrum. **28**, 403 (1957)] is carried out using complex analytic calculations and, inevitably, numerical solution of particle orbits. The results of this section will be applied to isochronous cyclotrons in Section 15.4. In principle, azimuthally varying fields could be used for focusing in accelerators with constant particle orbit radius, such as synchrotrons or betatrons. These configurations are usually referred to as FFAG (fixed-field, alternating-gradient) accelerators. In practice, the cost of magnets in FFAG machines is considerably higher than more conventional approaches, so AVF focusing is presently limited to cyclotrons.

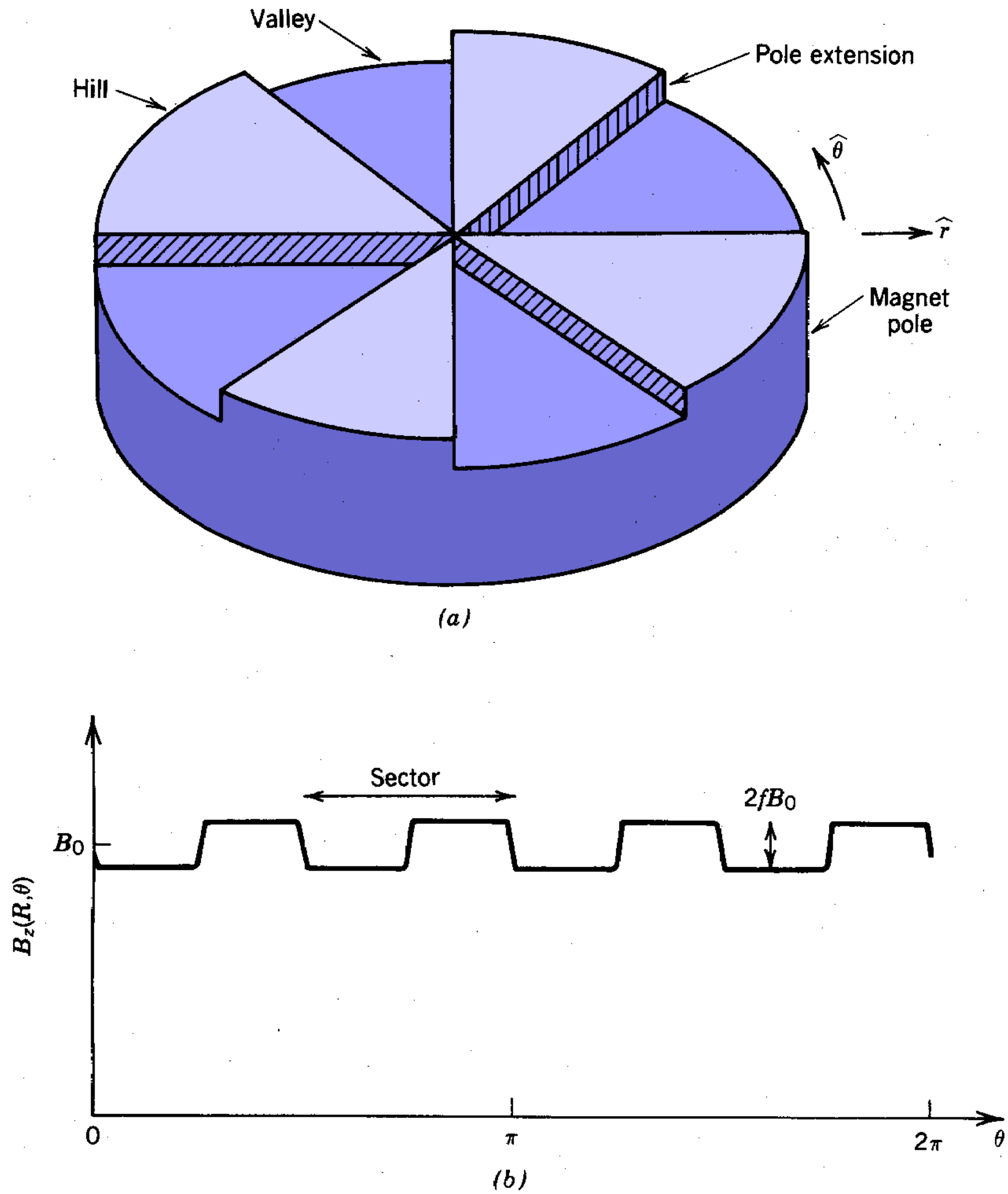

Figure 15.6 Magnetic fields in AVF cyclotron. (*a*) Magnet pole of AVF cyclotron, no spiral angle. (*b*) Vertical field amplitude as function of azimuth at constant radius.

Figure 15.6a illustrates an AVF cyclotron field generated by circular magnet poles with wedge-shaped extensions attached. We begin by considering extensions with boundaries that lie along diameters of the poles; more general extension shapes, such as sections with spiral boundaries, are discussed below. Focusing by fields produced by wedge-shaped extensions is usually referred to as *Thomas focusing* [L.H. Thomas, Phys. Rev. **54**, 580 (1938)]. The raised regions are called hills, and the recessed regions are called valleys. The magnitude of the vertical magnetic field is approximately inversely proportional to gap width; therefore, the field is stronger in hill regions. An element of field periodicity along a particle orbit is called a *sector*; a sector contains one hill and one valley. The number of sectors equals the number of pole extensions and is denoted N. Figure 15.6a shows a magnetic field with $N = 3$. The variation of magnetic with azimuth along a circle of radius R is plotted in Figure 15.6b. The definition of sector (as applied to the AVF cyclotron) should be noted carefully to avoid confusion with the term *sector magnet*.

The terminology associated with AVF focusing systems is illustrated in Figure 15.6b. The azimuthal variation of magnetic field is called *flutter*. Flutter is represented as a function of position by

$$B_z(R,\theta) = B_o(R)\ \Phi(R,\theta), \tag{15.18}$$

where $\Phi(R,\theta)$ is the *modulation function* which parametrizes the relative changes of magnetic field with azimuth. The modulation function is usually resolved as

$$\Phi(R,\theta) = 1 + f(R)\ g(\theta), \tag{15.19}$$

where $g(\theta)$ is a function with maximum amplitude equal to 1 and an average value equal to zero. The modulation function has a θ-averaged value of 1. The function $f(R)$ in Eq. (15.19) is the *flutter amplitude*.

The modulation function illustrated in Figure 15.6b is a step function. Other types of variation are possible. The magnetic field corresponding to a sinusoidal variation of gap width is approximately

$$B_z(R,\theta) = B_o(R)\ [1 + f(R)\ \sin N\theta], \tag{15.20}$$

so that

$$\Phi(\theta) = 1 + f(R)\ \sin N\theta. \tag{15.21}$$

The *flutter function* $F(R)$ is defined as the mean-squared relative azimuthal fluctuation of magnetic field along a circle of radius R:

$$F(R) = \overline{[(B_z(R,\theta) - B_o(R))/B_o(R)]^2} = (1/2\pi) \int_0^{2\pi} [\Phi(R,\theta) - 1]^2\ d\theta. \tag{15.22}$$

For example, $F(R) = f(R)^2$ for a step-function variation and $F(R) = ½\ f(R)^2$ for the sinusoidal variation of Eq. (15.21).

Particle orbits in azimuthally varying magnetic bending fields are generally complex. In order to develop an analytic orbit theory, simplifying assumptions will be adopted. We limit consideration

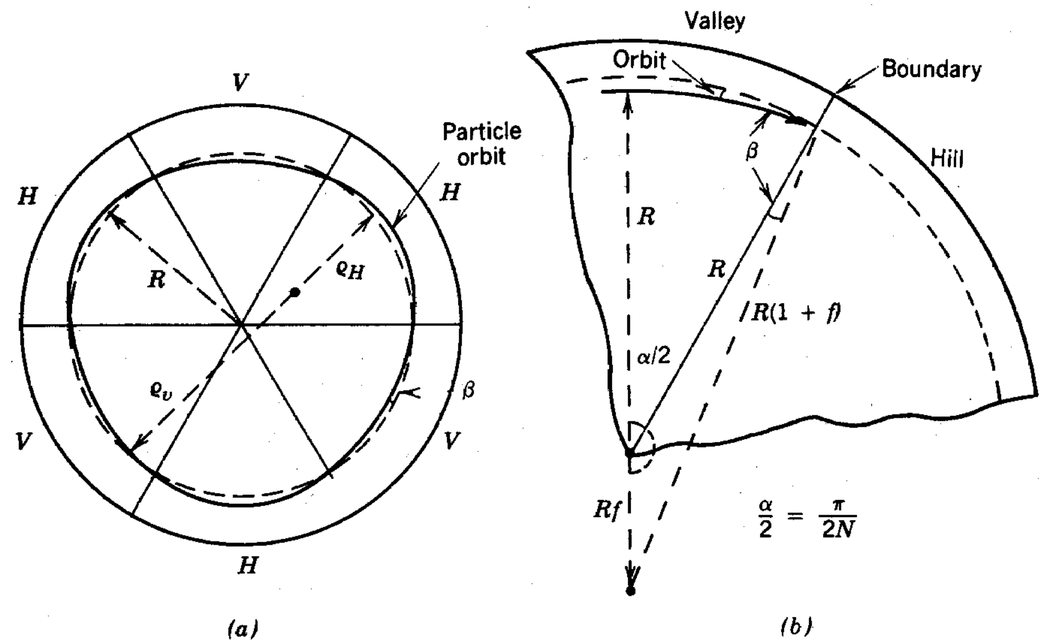

Figure 15.7 Thomas focusing with sharp field region boundaries in the limit of small flutter amplitude. (*a*) Main orbits: dashed line, uniform field; solid line, field with flutter. (*b*) Geometry for calculating focusing effect of fringing fields at valley–hill transition.

to a field with sharp transitions of magnitude between hills and valleys (Fig. 15.6b). The hills and valleys occupy equal angles. The step-function assumption is not too restrictive; similar particle orbits result from continuous variations of gap width. Two limiting cases will be considered to illustrate the main features of AVF focusing: (1) small magnetic field variations ($f \ll 1$) and (2) large field variations with zero magnetic field in the valleys. In the latter case, the bending field is produced by a number of separated sector magnets. Methods developed in Chapters 6 and 8 for periodic focusing can be applied to derive particle orbits.

To begin, take $f \ll 1$. As usual, the strategy is to find the equilibrium orbit and then to investigate focusing forces in the radial and vertical directions. The magnetic field magnitude is assumed independent of radius; effects of average field gradient will be introduced in Section 15.4. In the absence of flutter, the equilibrium orbit is a circle of radius $R = \gamma m_i c/qB_o$. With flutter, the equilibrium orbit is changed from the circular orbit to the orbit of Figure 15.7a. In the sharp field boundary approximation, the modified orbit is composed of circular sections. In the hill regions, the radius of curvature is reduced, while the radius of curvature is increased in the valley regions. The main result is that the equilibrium orbit is not normal to the field boundaries at the hill-valley transitions.

There is strong radial focusing in a bending field with zero average field index; therefore, flutter has little relative effect on radial focusing in the limit $f \ll 1$. Focusing in a cyclotron is conveniently characterized by the dimensionless parameter ν (see Section 7.2), the number of betatron wavelengths during a particle revolution. Following the discussion of Section 7.3, we find that

$$\nu_r^2 \cong 1 \tag{15.23}$$

for a radially uniform average field magnitude.

In contrast, flutter plays an important part in vertical focusing. Inspection of Figure 15.7a shows that the equilibrium orbit crosses between hill and valley regions at an angle to the boundary. The vertical forces acting on the particle are similar to those encountered in edge focusing (Section 6.9). The field can be resolved into a uniform magnetic field of magnitude $B_o[1 - f(R)]$ superimposed on fields of magnitude $2B_of(R)$ in the hill regions. Comparing Figure 15.7a to Figure 6.20, the orbit is inclined so that there is focusing at both the entrance and exit of a hill region. The vertical force arises from the fringing fields at the boundary; the horizontal field components are proportional to the change in magnetic field, $2B_of(R)$. Following Eq. 6.30, the boundary fields act as a thin lens with positive focal length

$$\textit{focal length} \cong (\gamma m_i c/q[2B_o f]) \;/\; |\tan\beta| \;=\; -R/2f\;|\tan\beta|, \tag{15.24}$$

where β is the angle of inclination of the orbit to the boundary. The ray transfer matrix corresponding to transit across a boundary is

$$\boldsymbol{A_b} = \begin{bmatrix} 1 & 0 \\ -2f\;\tan\beta/R & 1 \end{bmatrix} \tag{15.25}$$

The inclination angle can be evaluated from the geometric construction of Figure 15.7b. The equilibrium orbit crosses the boundary at about $r = R$. The orbit radii of curvature in the hill and valley regions are $R(1 \pm f)$. To first order, the inclination angle is

$$|\beta| = \pi f/2N, \tag{15.26}$$

where N is the number of sectors. The ray transfer matrix for a boundary is expressed as

$$\boldsymbol{A_b} = \begin{bmatrix} 1 & 0 \\ -\pi f^2/NR & 1 \end{bmatrix} \tag{15.26}$$

for small β. Neglecting variations in the orbit length through hills and valleys caused by the flutter, the transfer matrix for drift is

$$\boldsymbol{A_d} = \begin{bmatrix} 1 & \pi R/N \\ 0 & 1 \end{bmatrix} \tag{15.26}$$

A focusing cell, the smallest element of periodicity, consists of half a sector (a drift region and one boundary transition). The total ray transfer matrix is

$$\boldsymbol{A} = \begin{bmatrix} 1 & \pi R/N \\ -\pi f^2/NR & 1-½(\pi f/N)^2 \end{bmatrix} \tag{15.29}$$

The phase advance in the vertical direction is

$$\cos\mu \cong 1 - ½\mu^2 = ½Tr\boldsymbol{A} = 1 - ½(\pi f/N)^2, \tag{15.30}$$

or

$$\mu \cong \pi f/N. \tag{15.31}$$

The net phase advance during one revolution is equal to $2N\mu$. The number of betatron oscillations per revolution is therefore

$$\nu_z = 2N\mu/2\pi = f. \tag{15.32}$$

The final form is derived by substituting from Eq. (15.31). The vertical number of betatron wavelengths can also be expressed in terms of a flutter function as

$$\nu_z^2 = F. \tag{15.33}$$

Equation (15.33) is-not specific to a step-function field. It applies generally for all modulation functions.

Stronger vertical focusing results if the hill-valley boundaries are modified from the simple diametric lines of Figure 15.6. Consider, for instance, spiral-shaped pole extensions, as shown in Figure 15.8. At a radius R, the boundaries between hills and valleys are inclined at an angle $\zeta(R)$ with respect to a diameter. Spiral-shaped pole extensions lead to an additional inclination of magnitude $\zeta(R)$ between the equilibrium particle orbit and the boundary. The edge fields from the spiral inclination act to alternately focus and defocus particles, depending on whether the particle is entering or leaving a hill region. For example, the spiral of Figure 15.8 is defocusing at a hill-to-valley transition. A focusing-defocusing lens array provides net focusing.

The effect of boundary inclination can easily be derived in the limit that $f \ll 1$ and combined with Thomas focusing for a total ν_z. A focusing cell extends over a sector; a cell consists of a drift region of length $\pi R/N$, a thin lens of focal length $+2f\ \tan\zeta/R$, a second drift region, and a lens with focal length $-2f\ \tan\zeta/R$. The total ray transfer matrix for a sector is

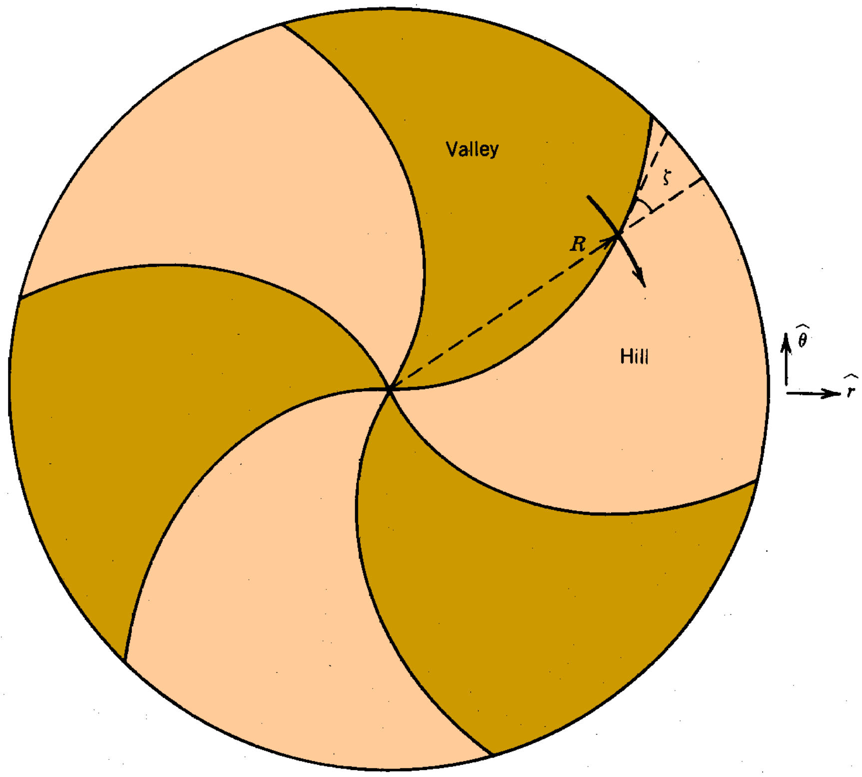

Figure 15.8 Geometry of magnet pole of spiral cyclotron showing inclination angle $\zeta(R)$.

$$\boldsymbol{A} = \begin{bmatrix} [1+2f\pi\ \tan\zeta/N-(2\pi f\ \tan\zeta/N)^2] & [2\pi R/N-2f\pi^2 R\ \tan\zeta/N^2] \\ [-4\pi f^2\ \tan^2\zeta/NR] & [1-2\pi f\ \tan\zeta/N] \end{bmatrix} \tag{15.34}$$

Again, identifying Tr**A** with $\cos\mu$, we find that

$$\mu \cong \sqrt{2}\pi f\ \tan\zeta\ /\ N. \tag{15.35}$$

Following the method used above, the number of vertical betatron oscillations per revolution is expressed simply as

$$\nu_z^2 = f^2\ (1 + 2\tan\zeta) = F\ (1 + 2\tan\zeta). \tag{15.36}$$

Vertical focusing forces can be varied with radius through the choice of the spiral shape. The Archimedean spiral is often used; the boundaries of the pole extensions are defined by

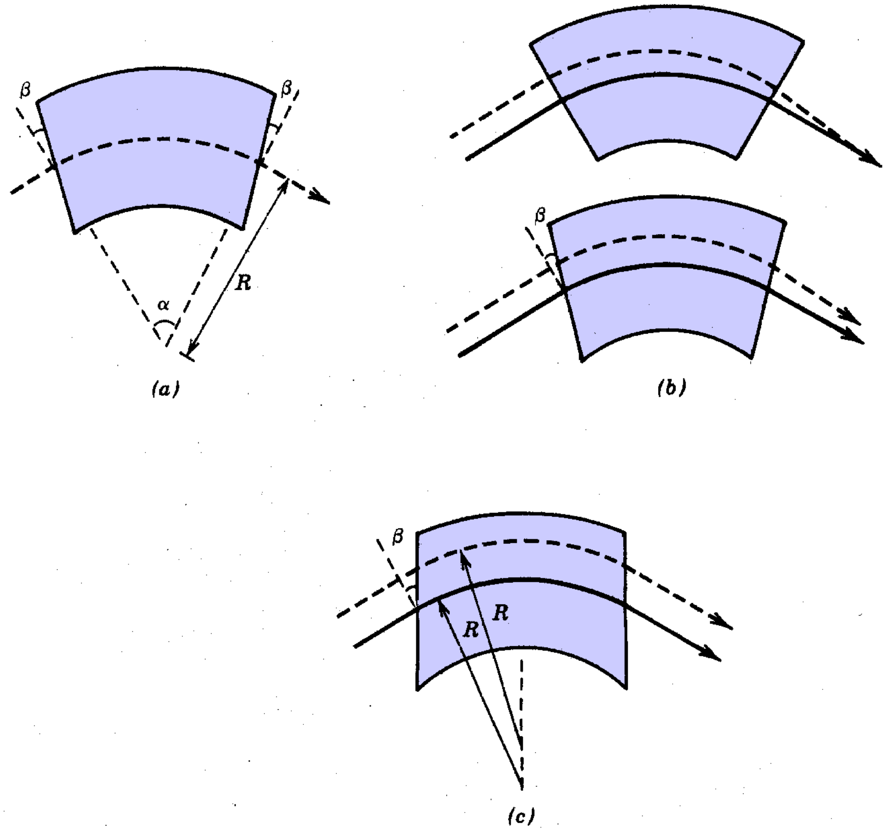

Figure 15.9 Focusing properties of a uniform field sector magnet with inclined boundaries. (a) Definition of angular extent of sector magnet (α) and boundary inclination angle (β) with respect to entering or exiting main particle orbit. (b) Horizontal trajectories of initially parallel particle orbits on main orbit (solid line) and displaced from main orbit (dashed line) with (bottom) and without (top) boundary inclination ($\beta < \frac{1}{2}\alpha$). ($c$) Horizontal orbits when $\beta = \frac{1}{2}\alpha$.

$$r = A\ [\theta + 2\pi J/2N], \tag{15.37}$$

where J = 0, 1, 2,...,$2N$ - 1. The corresponding inclination angle is

$$\tan\zeta(r) = d(r\theta)/dr = 2r/A. \tag{15.38}$$

Archimedean spiral pole extensions lead to vertical focusing forces that increase with radius.

An analytical treatment of AVF focusing is also possible for a step-function field with f = 1. In this case (corresponding to the separated sector cyclotron), the bending field consists of regions of uniform magnetic field separated by field-free regions. Focusing forces arise from the shape of the sector magnet boundaries. As an introduction, consider vertical and radial focusing in a single-sector magnet with inclined boundaries (Fig. 15.9a). The equilibrium orbit in the magnetic field region is a circular section of radius R centered vertically in the gap. The circular section subtends an angle α. Assume that the boundary inclinations, β, are equal at the entrance and exit of the magnet.

In the vertical direction, the ray transfer matrix for the magnet is the product of matrices representing edge focusing at the entrance, a drift distance αR, and focusing at the exit. We can apply Eqs. (15.27) and (15.28) to calculate the total ray transfer matrix. In order to calculate focusing in the radial direction, we must include the effect of the missing sector field introduced by the inclination angle P. For the geometry of Figure 15.9a, the inclination reduces radial focusing in the sector magnet. Orbits with and without a boundary inclination are plotted in Figure 15.9b. Figure 15.9c shows the equilibrium particle orbit and an off-axis parallel orbit in a sector magnet with $\beta = \frac{1}{2}\alpha$. The boundary is parallel to a line through the midplane of the magnet; the gyrocenters of both orbits also lie on this line. Therefore, the orbits are parallel throughout the sector and there is no focusing. A value of inclination $\beta < \frac{1}{2}\alpha$ moves the gyrocenter of the off-axis particle to the left; the particle emerges from the sector focused toward the axis. The limit on for radial focusing in a uniform-field sector magnet is

$$\beta = \tfrac{1}{2}\alpha \tag{15.39}$$

We now turn our attention to the AVF sector field with diametric boundaries shown in Figure 15.10. The equilibrium orbits can be constructed with compass and straightedge. The orbits are circles in the sector magnets and straight lines in between. They must match in position and angle at the boundaries. Figures 15.10a, b show solutions with $N = 2$ and $N = 3$ for hills and valleys occupying equal azimuths ($\alpha = \pi/N$). Note that in all cases the inclination angle of the orbit at a boundary is one-half the angular extent of the sector, $\beta = \frac{1}{2}\alpha$. Figures 15.10c and d illustrate the geometric construction of off-axis horizontal orbits for conditions corresponding to stability ($\alpha > \pi/N, \beta < \frac{1}{2}\alpha$) and instability ($\alpha < \pi/N, \beta > \frac{1}{2}\alpha$). The case of $N = 2$ is unstable for all choices of α. This arises because particles are overfocused when $\alpha > \pi/N$. This effect is clearly visible in Figure 15.10e. It is generally true that particle orbits are unstable in any type of AVF field with $N = 2$.

Spiral boundaries may also be utilized in separated sector fields. Depending on whether the particles are entering or leaving a sector, the edge-focusing effects are either focusing or defocusing in the vertical direction. Applying matrix algebra and the results of Section 6.9, it is easy to show that ν_z is

$$\nu_z^2 = (1 + 2\ \tan\zeta) \tag{15.40}$$

for $\alpha = \pi/N$. Spiral boundaries contribute alternate focusing and defocusing forces in the radial direction that are 180° out of phase with the axial forces. For $\alpha = \pi/N$, the number of radial betatron oscillations per revolution is approximately

$$\nu_r^2 \cong 2\ \tan\zeta. \tag{15.41}$$

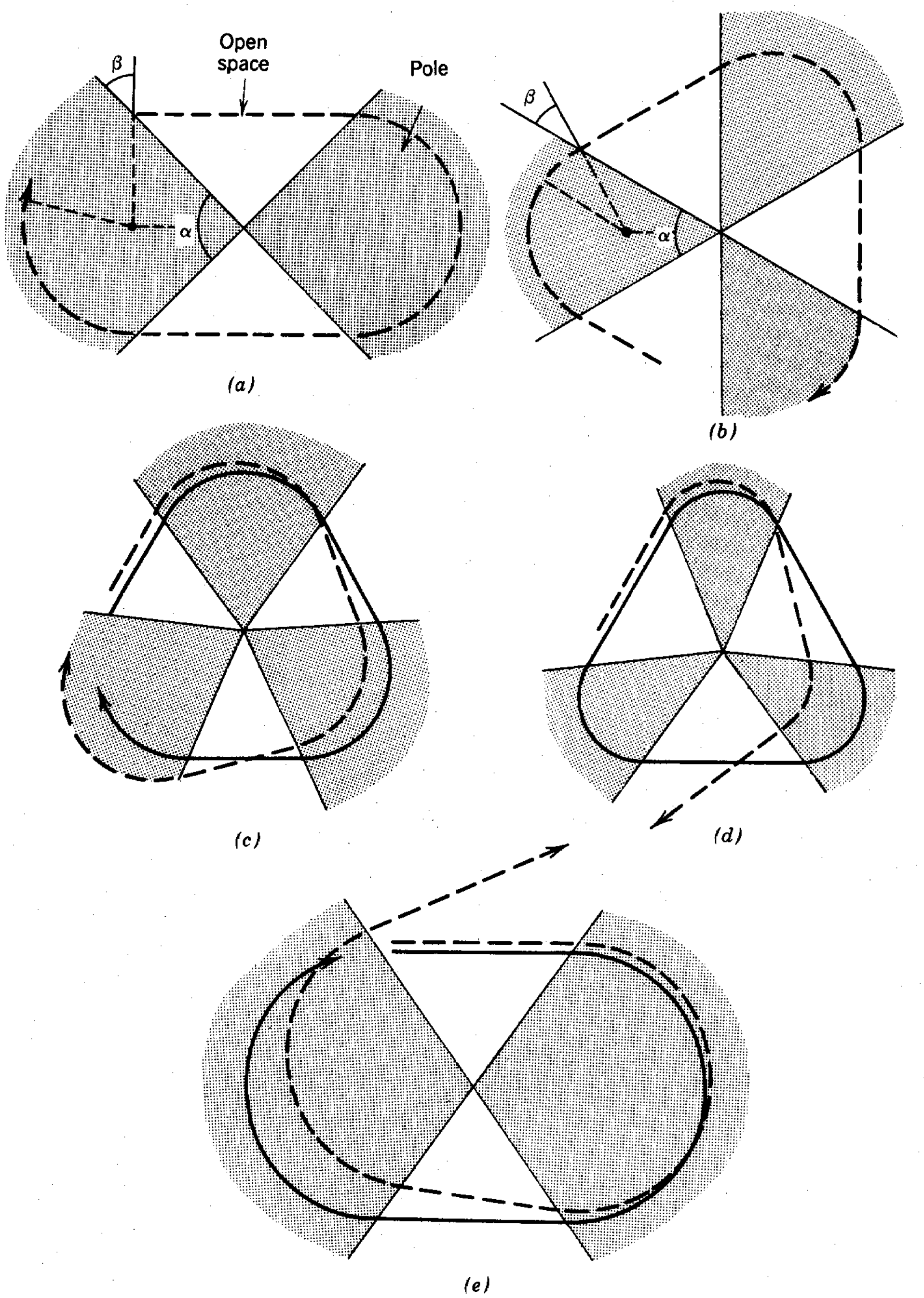

Figure 15.10 Horizontal particle orbits constructed with compass and straightedge in separated sector cyclotron with sector boundaries on diameter showing sector angular extent (α) and boundary inclination angle (β). (a) Main orbit with hills and valleys of equal angular extent ($\beta = \frac{1}{2}\alpha$), $N = 2$. (b) Main orbit with $\beta = \frac{1}{2}\alpha$, $N = 3$. (c) Stable horizontal orbits in three-sector field with $\beta < \frac{1}{2}\alpha$. Solid line, main orbit; dashed line, off-axis orbit. (d) Unstable horizontal orbits when $\beta > \frac{1}{2}\alpha$. ($e$) Illustration of instability in two-sector field with $\beta < \frac{1}{2}\alpha$.

15.4 THE SYNCHROCYCLOTRON AND THE AVF CYCLOTRON

Following the success of the uniform-field cyclotron, efforts were made to reach higher beam kinetic energy. Two descendants of the cyclotron are the synchrocyclotron and the AVF (isochronous) cyclotron. The machines resolve the problem of detuning between particle revolutions and rf field in quite different ways. Synchrocyclotrons have the same geometry as the SF cyclotron. A large magnet with circular poles produces an azimuthally symmetric vertical field with positive field index. Ions are accelerated from rest to high energy by an oscillating voltage applied between dees. The main difference is that the frequency is varied to preserve synchronism.

There are a number of differences in the operation of synchrocyclotrons and cyclotrons. Synchrocyclotrons are cycled, rather than continuous; therefore, the time-average beam current is much lower. The longitudinal dynamics of particles in a synchrocyclotron do not follow the model of Section 15.2 because there is a synchronous phase. The models for phase dynamics developed in Chapter 13 can be adapted to the synchrocyclotron. The machine can contain a number of confined particle bunches with phase parameters centered about the bunch that has ideal matching to the rf frequency. The beam bunches are distributed as a group of closely spaced turns of slightly different energy. The acceptance of the rf buckets decreases moving away from the ideal match, defining a range of time over which particles can be injected into the machine. In research applications, the number of bunches contained in the machine in a cycle is constrained by the allowed energy spread of the output beam.

There are technological limits on the rate at which the frequency of oscillators cpn be swept. These limits were particularly severe in early synchrocyclotrons that used movable mechanical tuners rather than the ferrite tuners common on modern synchrotrons. The result is that the acceleration cycle of a synchrocyclotron extends over a longer period than the acceleration time for an ion in a cyclotron. Typically, ions perform between 10,000 and 50,000 revolutions during acceleration in a synchrocyclotron. The high recirculation factor implies lower voltage between the dees. The cycled operation of the synchrocyclotron leads to different methods of beam extraction compared to cyclotrons. The low dee voltage implies that orbits have small separation (< 1 mm), ruling out the use of a septum. On the other hand, all turns can be extracted at the same time by a pulsed field because they are closely spaced in radius. Figure 15.11 illustrates one method of beam extraction from a synchrocyclotron. A pulsed electric field is used to deflect ions on to a perturbed orbit which leads them to a magnetic shield. The risetime of voltage on the kicker electrodes should be short compared to the revolution time of ions. Pulsed extraction is characteristic of cycled machines like the synchrocyclotron and synchrotron. In large synchrotrons with relatively long revolution time, pulsed magnets with ferrite cores are used for beam deflection.

Containment of high-energy ions requires large magnets. For example, a 600-MeV proton has a gyroradius of 2.4 m in a 1.5-T field. This implies a pole diameter greater than 15 ft. Synchro-cyclotron magnets are among the largest monolithic, iron core magnets ever built. The limitation of this approach is evident; the volume of iron required rises roughly as the cube of the kinetic energy. Two synchrocyclotrons are still in operation: the 184-in. machine at Lawrence Berkeley Laboratory and the CERN SC.

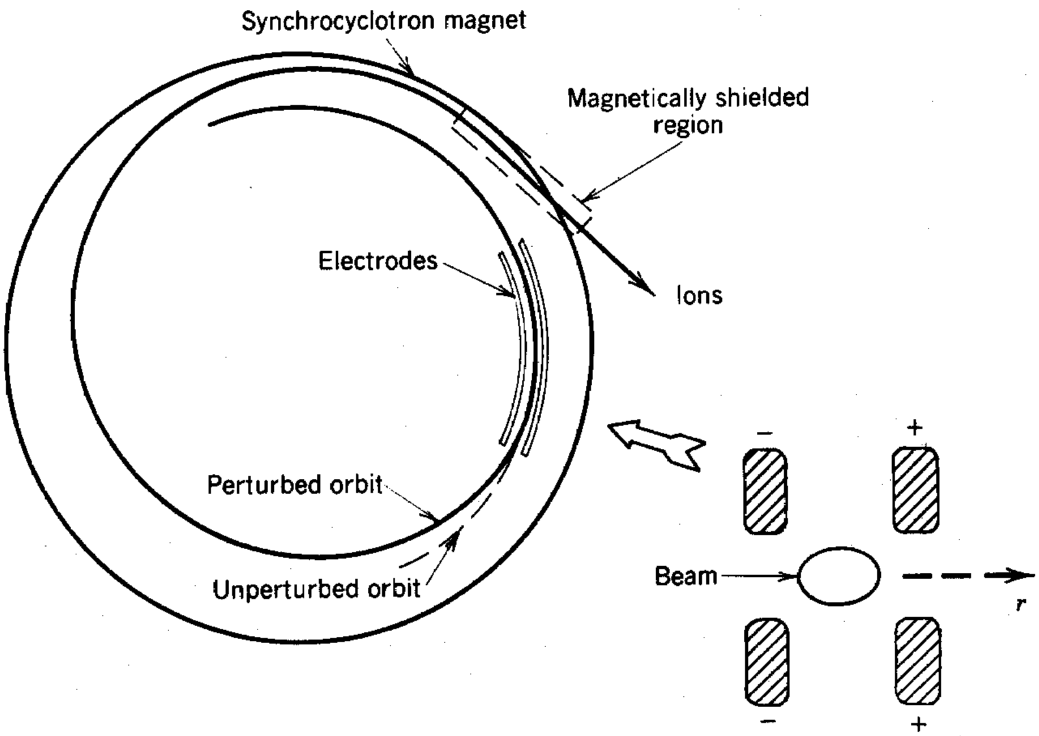

Figure 15.11 Beam extraction from a synchrocyclotron by a pulsed radial electric field.

The AVF cyclotron has fixed magnetic field and rf frequency; it generates a continuous-beam pulse train. Compensation for relativistic mass increase is accomplished by a magnetic field that increases with radius. The vertical defocusing of the negative field index is overcome by the focusing methods described in Section 15.3.

We begin by calculating the radial field variations of the θ-averaged vertical field necessary for synchronization. The quantity $B(R)$ is the averaged field around a circle of radius R and B_o is the field at the center of the machine. Assume that flutter is small, so that particle orbits approximate circles of radius R, and let $B(R)$ represent the average bending field at R. Near the origin ($R = 0$), the AVF cyclotron has the same characteristics as a uniform field cyclotron; therefore, the rf frequency is

$$\omega = qB_o/m_i, \tag{14.42}$$

where m_i is the rest energy of the ion. Synchronization with the fixed frequency at all radii implies that

$$B(R) = \gamma(R)m_i\omega/q, \tag{15.43}$$

or

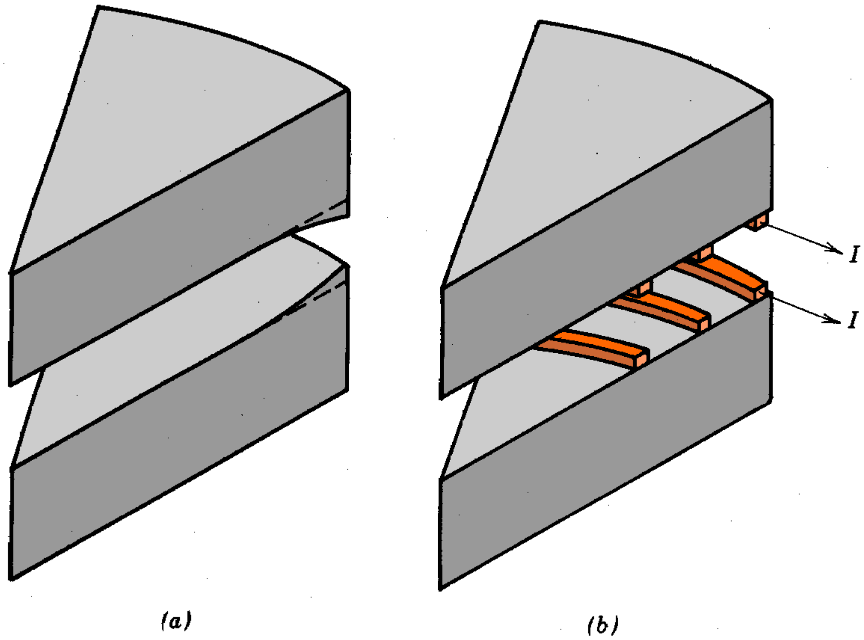

Figure 15.12 Methods for generating vertical magnetic field with negative field index (positive radial gradient). (*a*) Radial variation of gap width. (*b*) Trim coils.

$$B(R)/B_o = \gamma(R). \tag{15.44}$$

The average magnetic field is also related to the average orbit radius and ion energy through Eq. (3.38):

$$R = \frac{\gamma(R)\ \beta m_i c}{qB(R)} = \frac{m_i c}{qB(R)} \sqrt{\gamma^2 - 1} = \frac{m_i c}{qB_o} \frac{\sqrt{\gamma^2 - 1}}{\gamma} . \tag{15.45}$$

Combining Eqs. (15.44) and (15.45), we find

$$B(R)/B_o = \gamma(R) = \sqrt{1 - (qB_o R/m_i c^2)^2} . \tag{15.46}$$

Equation (15.46) gives the following radial variation of the field index:

$$n(R) = - [R/B(R)]\ [dB(R)/dR] = - (\gamma^2 - 1). \tag{15.47}$$

Two methods for generating a bending field with negative field index (positive radial gradient) are illustrated in Figure 15.12. In the first, the distance between poles decreases as a function of radius. This method is useful mainly in small, low-energy cyclotrons. It has the following drawbacks for large research machines:

1. The constricted gap can interfere with the dees.

2. The poles must be shaped with great accuracy.

3. A particular pole shape is suitable for only a single type of ion.

A better method to generate average radial field gradient is the use of *trimming coils*, illustrated in Figure 15.12b. Trimming coils (or k coils) are a set of adjustable concentric coils located on the pole pieces inside the magnet gap. They are used to shift the distribution of vertical field. With adjustable trimming coils, an AVF cyclotron can accelerate a wide range of ion species.

In the limit of small flutter amplitude ($f \ll 1$), the radial and vertical betatron oscillations per revolution in an AVF cyclotron are given approximately by

$$\nu_r^2 \cong 1 - n + F(R)n^2/N^2 + \ldots, \qquad (15.48)$$

$$\nu_z^2 \cong n + F(R) + 2F(R)\tan^2\zeta + F(R)n^2/N^2 + \ldots. \qquad (15.49)$$

Equations (15.48) and (15.49) are derived through a linear analysis of orbits in an AVF field in the small flutter limit. The terms on the right-hand side represent contributions from various types of focusing forces. In Eq. (15.48), the terms have the following interpretations:

Term 1: Normal radial focusing in a bending field.

Term 2: Contribution from an average field gradient ($n < 0$ in an AVF cyclotron).

Term 3: Alternating-gradient focusing arising from the change in the actual field index between hills and valleys. Usually, this is a small effect.

A term involving the spiral angle ζ is absent from the radial equation. This comes about because of cancellation between the spiral term and a term arising from differences of the centrifugal force on particles between hills and valleys.

The terms on the right-hand side of Eq. (15.49) for vertical motion represent the following contributions:

Term 1: Defocusing by the average radial field gradient.

Term 2: Thomas focusing.

Term 3: FD focusing by the edge fields of a spiral boundary.

Term 4: Same as the third term of Eq. (15.48).

Symmetry considerations dictate that the field index and spiral angle near the center of an AVF cyclotron approach zero. The flutter amplitude also approaches zero at the center because the effects of hills and valleys on the field cancel out at radii comparable to or less than the gap width between poles. As in the conventional cyclotron, electrostatic focusing at the acceleraton gaps plays an important role for vertical focusing of low-energy ions. At large radius, there is little problem in ensuring good radial focusing. Neglecting the third term, Eq. (15.48) may be rewritten as

$$\nu_r \cong \gamma \tag{15.50}$$

using Eq. (15.47). The quantity ν_r is always greater than unity; radial focusing is strong. Regarding vertical focusing, the combination of Thomas focusing and spiral focusing in Eq. (15.49) must increase with radius to compensate for the increase in field index. This can be accomplished by a radial increase of $F(R)$ or $\zeta(R)$. In the latter case, boundary curves with increasing ζ (such as the Archimedean spiral) can be used. Isochronous cyclotrons have the property that the revolution time is independent of the energy history of the ions. Therefore, there are no phase oscillations, and ions have neutral stability with respect to the rf phase. The magnet poles of high-energy isochronous cyclotrons must be designed with high accuracy so that particle synchronization is maintained through the acceleration process.

In addition to high-energy applications, AVF cyclotrons are well suited to low-energy medical and industrial applications. The increased vertical focusing compared to a simple gradient field means that the accelerator has greater transverse acceptance. Higher beam currents can be contained, and the machine is more tolerant to field errors (see Section 15.7). Phase stability is helpful, even in low-energy machines. The existence of a synchronous phase implies higher longitudinal acceptance and lower beam energy spread. The AVF cyclotron is much less expensive per ion produced than a uniform-field cyclotron.

In the range of kinetic energy above 100 MeV, the separated sector cyclotron is a better choice than the single-magnet AVF cyclotron. The separated sector cyclotron consists of three or more bending magnets separated by field-free regions. It has the following advantages:

1. Radio-frequency cavities for beam acceleration can be located between the sectors rather than between the magnet poles. This allows greater latitude in designing the focusing magnetic field and the acceleration system. Multiple acceleration gaps can be accommodated, leading to rapid acceleration and large orbit separation.

2. The bending field is produced by a number of modular magnets rather than a single larger unit. Modular construction reduces the problems of fabrication and mechanical stress. This is particularly important at high energy.

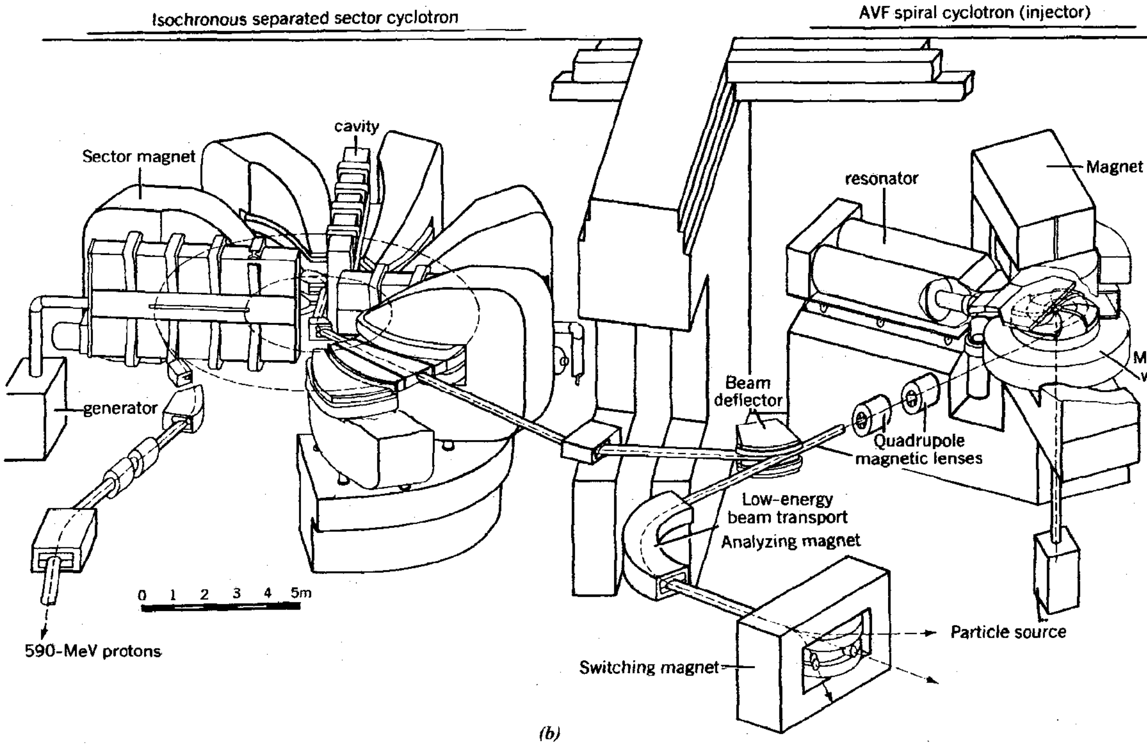

(b)

Figure 15.13 SIN Cyclotron. (*a*) Scale drawing, showing injector AVF cyclotron with spiral extensions of magnet pole and separated sector cyclotron with spiral field boundaries. (*b*) Overhead view of field boundaries in separated sector cyclotron with calculated proton orbits at 75, 177, 279, 381, 483, and 585 MeV. (Courtesy W. Joho, Swiss Institute for Nuclear Studies.)

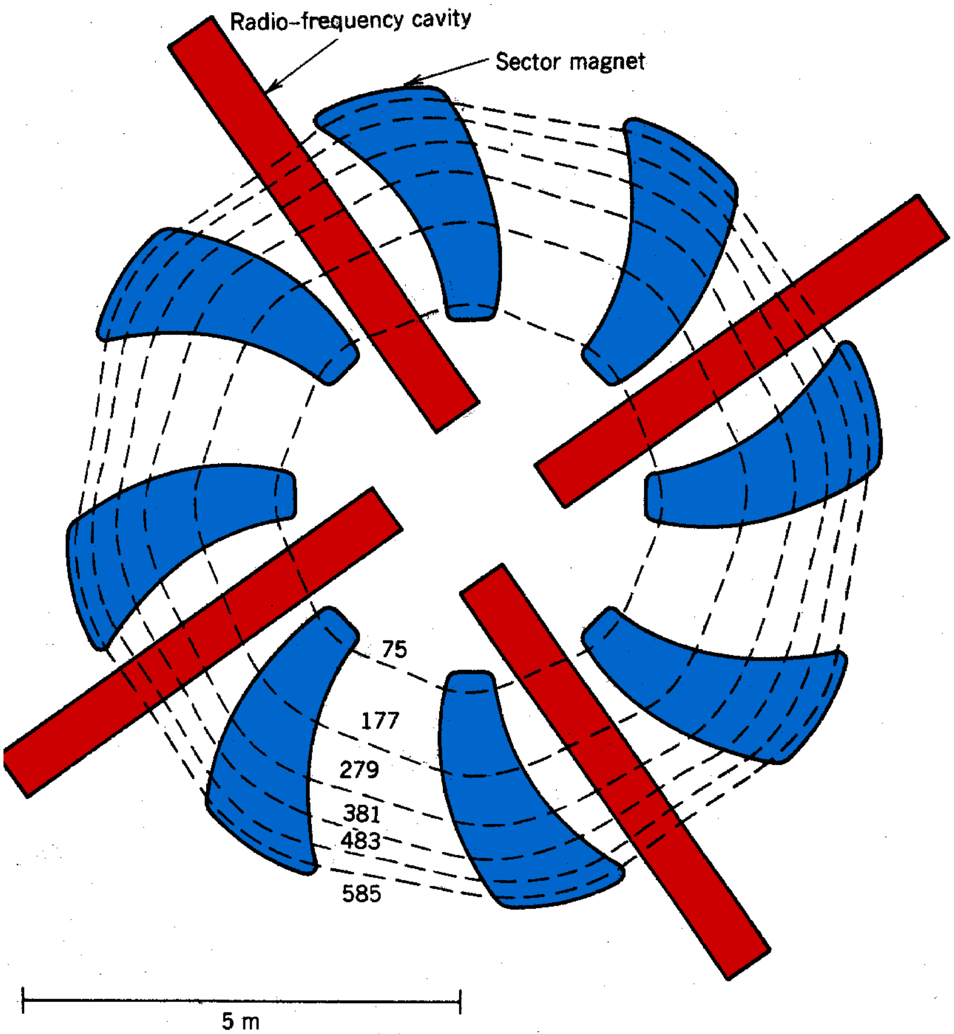

(b)

Figure 15.13 (*Continued*)

The main drawback of the separated sector cyclotron is that it cannot accelerate ions from zero energy. The beam transport region is annular because structures for mechanical support of the individual magnet poles must be located on axis. Ions are pre-accelerated for injection into a separated sector cyclotron. Pre-acceleration can be accomplished with a low-energy AVF cyclotron or a linac. The injector must be synchronized so that micropulses are injected into the high-energy machine at the proper phase.

Figure 15.13a shows the separated sector cyclotron at the Swiss Nuclear Institute. Parameters of the machine are summarized in Table 15.1. The machine was designed for a high average flux of light ions to generate mesons for applications to radiation therapy and nuclear research. The accelerator has eight spiral sector magnets with a maximum hill field of 2.1 T. Large waveguides

TABLE 15.1 Parameters of SIN 590 MeV Cyclotron[a]

Injector Cyclotron	
Configuration	AVF cyclotron with spiral-shaped sectors
Injection radius	1.5 cm
Extraction radius	105 cm
Pole diameter	250 cm
Peak magnetic field	1.65 T
Number of sectors	4
Maximum spiral angle	55°
Number of trimming coils	12
Magnet power	500 kW
Number of dees	1
rf frequency	4.6–17 MHz (tunable)
Maximum energy gain/turn	160 kV/turn
Beam energy (protons)	10–72 MeV
Beam current (protons)	170 μA
590-MeV Separated Sector Cyclotron	
Main applications	Research in nuclear physics, solid-state physics and chemistry, pion therapy
Injection radius	210 cm
Extraction radius	445 cm
Peak magnetic field	2.09 T
Averaged field at exit radius	0.87 T
Number of sector magnets	8
Maximum spiral angle	35°
Number of trimming coils	18
Magnet power	670 MW
Number of acceleration cavities	4
rf frequency	50.63 MHz
Maximum energy gain/turn	2200 kV/turn
rf power (maximum)	800 MW
Extraction system	Electrostatic septum

[a]Swiss Nuclear Research Institute.

connect rf supplies to a four acceleration gaps. In operation, the machine requires 0.5 MW of rf input power. The peak acceleration gap voltage is 500 kV. The maximum orbit diameter of the cyclotron is 9 in for a maximum output energy of 590 MeV (protons). The time-averaged beam current is 200 μA. A standard AVF cyclotron with four spiral-shaped sectors is used as an injector. An increase of average beam current to 1 mA is expected with the addition of a new injector. The injector is a spiral cyclotron with four sectors. The injector operates at 50.7 MHz and generates 72-MeV protons. Figure 15.13b is an overhead view of the magnets and rf cavities in the separated sector cyclotron. Six selected orbits are illustrated at equal energy intervals from 72 to 590 MeV. Note that the distance an ion travels through the sector field increases with orbit radius (negative effective field index). The diagram also indicates the radial increase of the inclination angle between sector field boundaries and the particle orbits.

15.5 PRINCIPLES OF TliE SYNCHROTRON

Synchrotrons are resonant circular particle accelerators in which both the magnitude of the bending magnetic field and the rf frequency are cycled. An additional feature of most modem synchrotrons is that focusing forces are adjustable independent of the bending field. Independent variation of the focusing forces, beam-bending field, and rf frequency gives synchrotrons two capabilities that lead to beam energies far higher than those from other types of circular accelerators:

1. The betatron wavelength of particles can be maintained constant as acceleration proceeds. This makes it possible to avoid the orbital resonances that limit the output energy of the AVF cyclotron.

2. The magnetic field amplitude is varied to preserve a constant particle orbit radius during acceleration. Therefore, the bending field need extend over only a small annulus rather than fill a complete circle. This implies large savings in the cost of the accelerator magnets. Furthermore, the magnets can be fabricated as modules and assembled into ring accelerators exceeding 6 km in circumference.

The main problems of the synchrotron are (1) a complex operation cycle and (2) low average flux.

The components of a modem separated function synchrotron are illustrated in Figure 15.14. An ultra-high-vacuum chamber for beam transport forms a closed loop. Circular sections may be interrupted by straight sections to facilitate beam injection, beam extraction, and experiments. Acceleration takes place in a cavity filled with ferrite cores to provide inductive iso a over a broad frequency range. The cavity is similar to a linear induction accelerator cavity. The two differences are (1) an ac voltage is applied across the gap and (2) the ferrites are not driven to saturation to minimize power loss.

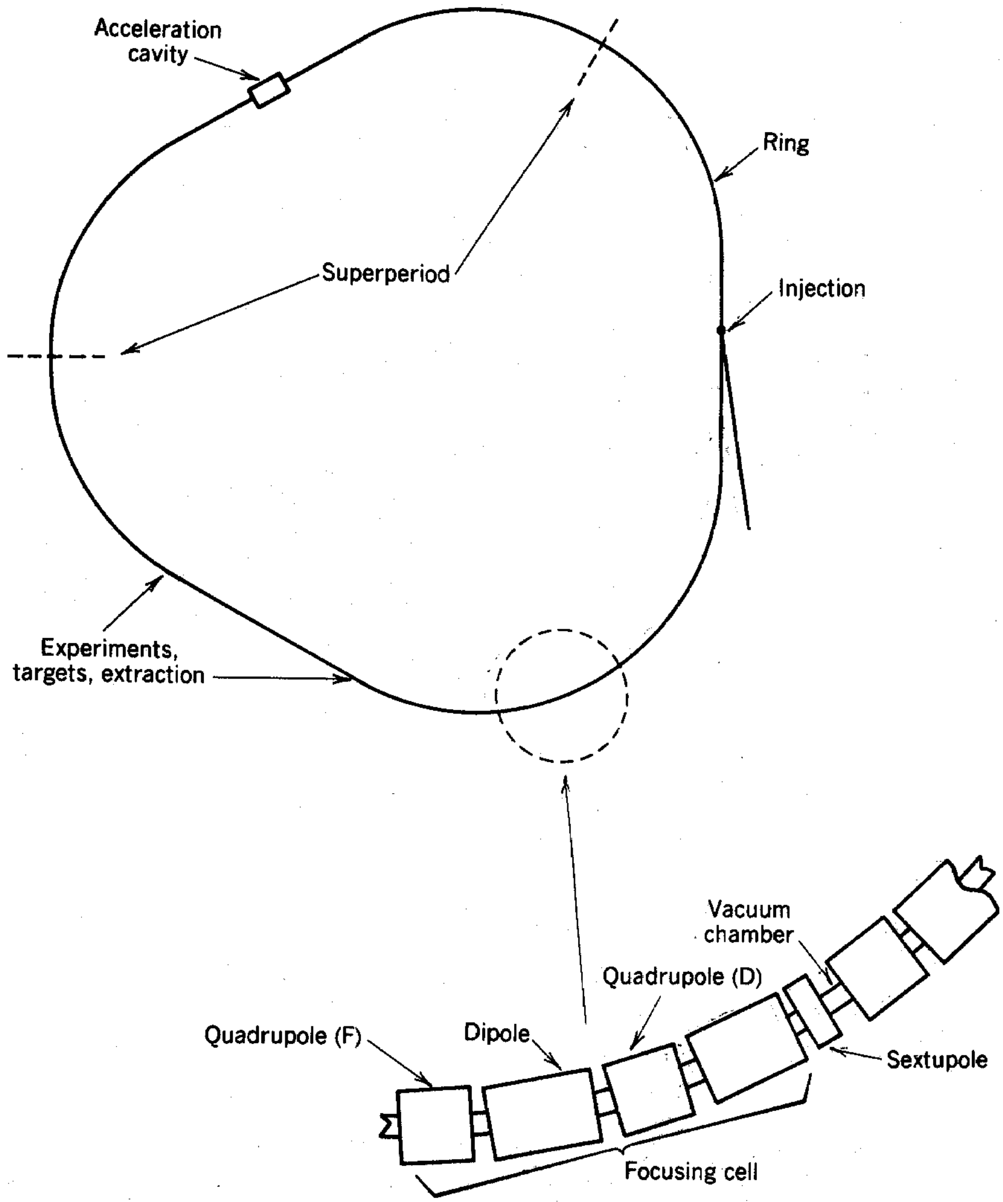

Figure 15.14 Major components and definition of terms in separated function synchrotron.

Beam bending and focusing are accomplished with magnetic fields. The separated function synchrotron usually has three types of magnets, classified according to the number of poles used to generate the field. *Dipole magnets* (Fig. 15.15a) bend the beam in a closed orbit. *Quadrupole magnets* (Fig. 15.15b) (grouped as quadrupole lens sets) focus the beam. *Sextupole magnets* (Fig. 15.15c) are usually included to increase the tolerance of the focusing system to beam energy spread. The global arrangement of magnets around the synchrotron is referred to as a *focusing lattice*. The lattice is carefully designed to maintain a stationary beam envelope. In order to avoid

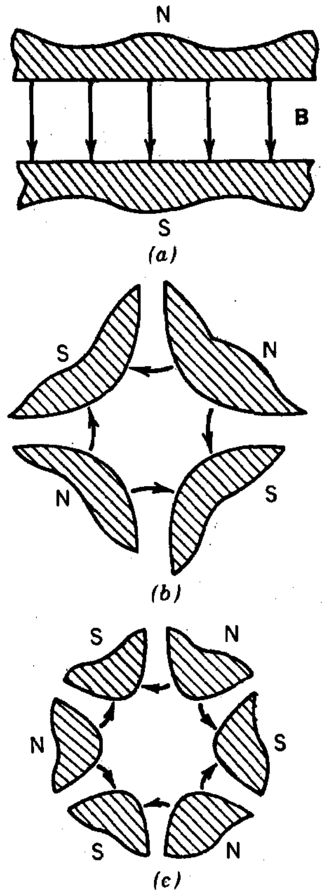

Figure 15.15 Classification of synchrotron magnets. (*a*) Dipole magnet (bending particle orbits). (*b*) Quadrupole (transverse focusing). (*c*) Sextupole (chromatic correction; assuring that particles in a range of energy about the mean have the same ν).

resonance instabilities, the lattice design must not allow betatron wavelengths to equal a characteristic dimension of the machine (such as the circumference). Resonance conditions are parametrized in terms of *forbidden values* of ν_r and ν_z.

A focusing cell is strictly defined as the smallest element of periodicity in a focusing system. A period of a noncircular synchrotron contains a large number of optical elements. A cell may encompass a curved section, a straight section, focusing and bending magnets, and transition elements between the sections. The term *superperiod* is usually used to designate the minimum periodic division of a synchrotron, while focusing cell is applied to a local element of periodicity within a superperiod. The most common local cell configuration is the *FODO* cell. It consists of a focusing quadrupole (relative to the *r* or *z* direction), a dipole magnet, a defocusing quadrupole, and another dipole. Horizontal focusing forces in the bending magnets are small compared to that in the quadrupoles. For transverse focusing, the cell is represented as a series of focusing and defocusing lenses separated. by drift (open) spaces.

The alternating-gradient synchrotron (AGS) is the precursor of the separated function synchrotron. The AGS has a ring of magnets which combine the functions of beam bending and focusing. Cross sections of AGS magnets are illustrated in Figure 15.16. A strong positive or

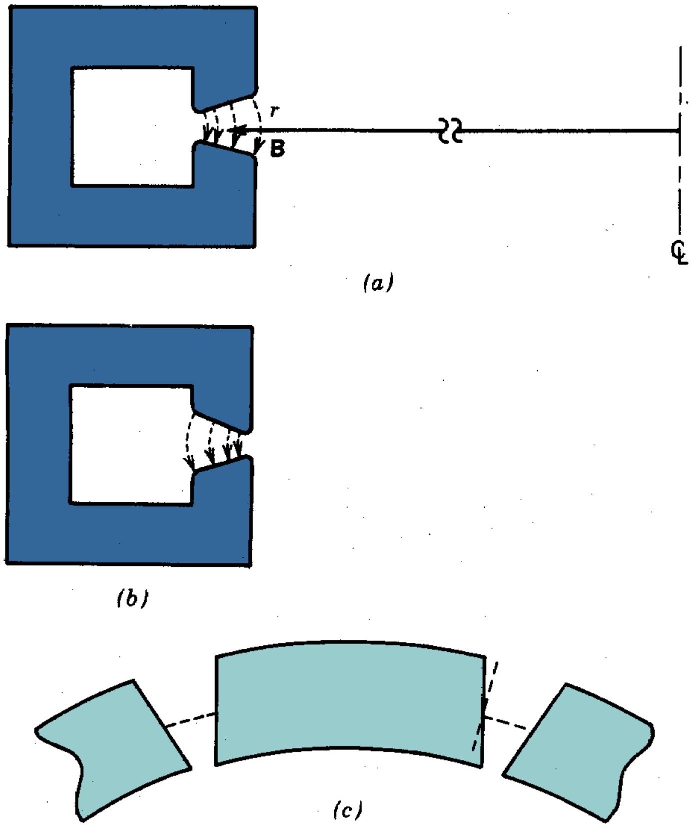

Figure 15.16 Synchrotron Magnets. (*a*) Magnet in alternating-gradient synchrotron with strong radial focusing and vertical defocusing. (*b*) AGS magnet with strong vertical focusing and radial defocusing. (*c*) Overhead view of uniform-field sector magnet boundaries in zero-gradient synchrotron.

negative radial gradient is superimposed on the bending field; horizontal and vertical focusing arises from the transverse fields associated with the gradient (Section 7.3). The magnet of Figure 15.16a gives strong radial focusing and horizontal defocusing, while the opposite holds for the magnet of Figure 15.16b.

Early synchrotrons utilized simple gradient focusing in an azimuthally symmetric field. They were constructed from a number of adjacent bending magnets with uniform field index in the range $0 < n < 1$. These machines are now referred to as *weak focusing synchrotrons* because the betatron wavelength of particles was larger than the machine circumference. The zero-gradient synchrotron (ZGS) (Fig. 15.16c) was an interesting variant of the weak focusing machine. Bending and focusing were performed by sector magnets with uniform-field magnitude (zero gradient). The sector field boundaries were inclined with respect to the orbits to give vertical focusing [via edge focusing (Section 6.9)] and horizontal focusing [via sector focusing (Section 6.8)]. The advantage of the ZGS compared to other weak focusing machines was that higher bending fields could be achieved without local saturation of the poles.

The limit on kinetic energy in an ion synchrotron is set by the bending magnetic field magnitude and the area available for the machine. The ring radius of relativistic protons is given by

$$R = 3.3E/\overline{B} \quad (m), \tag{15.51}$$

where $\overline{B}$ is the average magnetic field (in tesla) and E is the total ion energy in GeV. Most ion synchrotrons accelerate protons; protons have the highest charge-to-mass ratio and reach the highest kinetic energy per nucleon for a given magnetic field. Synchrotrons have been used for heavy-ion acceleration. In this application, ions are pre-accelerated in a linear accelerator and directed through a thin foil to strip electrons. Only ions with high charge states are selected for injection into the synchrotron.

The maximum energy in an electron synchrotron is set by emission of *synchrotron radiation*. Synchrotron radiation results from the continuous transverse acceleration of particles in a circular orbit. The total power emitted per particle is

$$P = 2cE^4 r_o/3R^2(m_o c^2)^3 \quad (watts), \tag{15.52}$$

where E is the total particle energy and R is the radius of the circle. Power in Eq. (15.52) is given in electron volts per second if all energies on the right-hand side are expressed in electron volts. The quantity r_o is the classical radius of the particle,

$$r_o = q^2/4\pi\varepsilon_o m_o c^2. \tag{15.53}$$

The classical radius of the electron is

$$r_e = 2.82 \times 10^{-15} \ m. \tag{15.54}$$

Inspection of Eqs. (15.52) and (15.53) shows that synchrotron radiation has a negligible effect in ion accelerators. Compared to electrons, the power loss is reduced by a factor of $(m_e/m_i)^4$. To illustrate the significance of synchrotron radiation in electron accelerators, consider a synchrotron in which electrons gain an energy eV_o per turn. The power input to electrons (in eV/s) is

$$P = cV_o/2\pi R. \tag{15.55}$$

Setting Eqs. (15.52) and (15.55) equal, the maximum allowed total energy is

$$E \leq [3V_o(m_o c^2)^3 R/4\pi r_o]^{0.25}. \tag{15.56}$$

For example, with R = 20 m and V_o = 100 kV, the maximum energy is E = 2.2 GeV. Higher energies result from a larger ring radius and higher power input to the accelerating cavities, but the scaling is weak. The peak energy achieved in electron synchrotrons is about 12 GeV for R = 130 m. Linear accelerators are the only viable choice to reach higher electron energy for particle physics research. Nonetheless, electron synchrotrons are actively employed in other areas of applied physics research. They are a unique source of intense radiation over a wide spectral range via synchrotron radiation. New synchrotron radiation facilities are planned as research tools in atomic and solid-state physics.

Synchrotron radiation has some advantageous effects on electron beam dynamics in synchrotrons. The quality of the beam (or the degree to which particle orbit parameters are identical) is actually enhanced by radiation. Consider, for instance, the spread in longitudinal energy in a beam bunch. Synchrotron radiation is emitted over a narrow cone of angle

$$\Delta\theta = (m_e c^2/E) \tag{15.57}$$

in the forward direction relative to the instantaneous electron motion. Therefore, the emission of photons slows electrons along their main direction of motion while making a small contribution to transverse motion. According to Eq. (15.52), higher-energy electrons lose more energy; therefore, the energy spread of an electron bunch decreases. This is the simplest example of beam cooling. The process results in a reduction of the random spread of particle orbits about a mean; hence, the term *cooling*.

The highest-energy accelerator currently in operation is located at the Fermi National Accelerator Laboratory. The 2-km-diameter proton synchrotron consists of two accelerating rings, built in two stages. In the main ring (completed in 1971), beam focusing and bending are performed by conventional magnets. Beam energies up to 450 GeV have been achieved in this ring. After seven years of operation, an additional ring was added in the tunnel beneath the main ring. This ring, known as the energy doubler, utilizes superconducting magnets. The higher magnetic field makes it possible to generate beams with 800 GeV kinetic energy. The total experimental facility, with beam transport elements and experimental areas designed to accommodate the high-energy beams, is known as the Tevatron. A scale drawing of the accelerator and experimental areas is shown in Figure 15.17a. Protons, extracted from a 750-kV electrostatic accelerator, are accelerated in a 200-MeV linear accelerator. The beam is then injected into a rapid cycling booster synchrotron which increases the energy to 8 GeV. The booster synchrotron cycles in 33 ms. The outputs from 12 cycles of the booster synchrotron are used to fill the main ring during a constant-field initial phase of the main ring acceleration cycle. The booster synchrotron has a circumference equal to 1/13.5 that of the main ring. The 12 pulses are injected head to tail to fill most of the main ring circumference.

A cross section of a superconducting bending magnet from the energy doubler is shown in Figure 15.17b. It consists of a central bore tube of average radius 7 cm surrounded by superconducting windings with a spatial distribution calculated to give a highly uniform bending field. The windings are surrounded by a layer of stainless steel laminations to clamp the windings

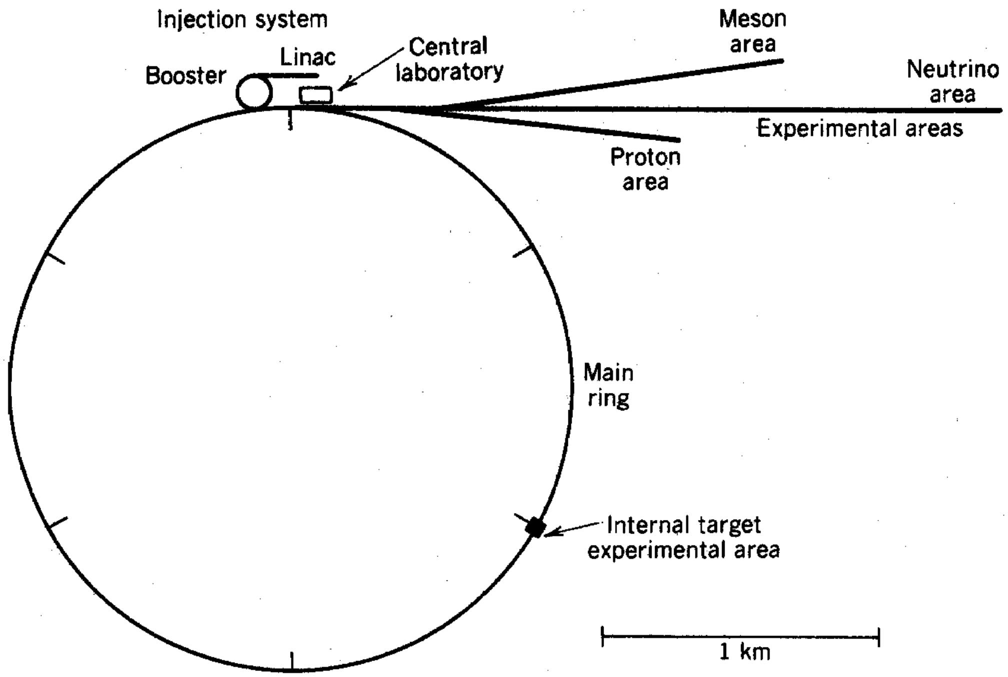

(a)

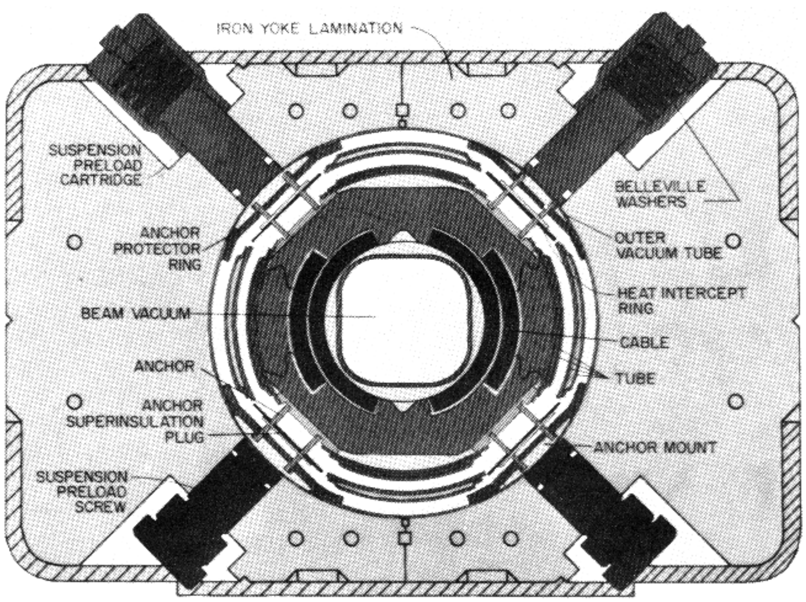

(b)

Figure 15.17 FNAL Synchrotron. (*a*) Scale over head view showing injector accelerators, main accelerator ring, and experimental areas for elementary particle physics research. (*b*) Cross-sectional view energy doubler superconducting bending magnet. (Courtesy F. Cole, Fermi National Accelerator Laboratory.)

TABLE 15.2 Parameters of 400-GeV Synchrotron[a]

	Injector
Beam energy	750 keV
Particle	p^+
Beam current	200 mA
	Linac
Beam energy	200 MeV
Beam current	100 mA
Beam macropulselength	3–12 μs
Length	140 m
Configuration	Drift tube linac
Number of drift tubes	295
Frequency	200 MHz
	Booster Synchrotron
Radius	74.1 m
Beam energy	8 GeV
Cycle time	0.067 s
Peak magnetic field	0.7 T
Energy gain/turn	0.7 MeV/turn
Configuration	Alternating gradient, H-type magnets
Number of magnets	96
Pulse rate	15 Hz
Number of rf cavities	16
Frequency excursion	30–53 MHz
Transition energy	4.2 GeV
Peak intensity	10^{12} protons/pulse
	Main Ring
Configuration	Separated function, bending dipole magnets, and quadrupole focusing magnets
Number of magnets	1014
Peak magnetic field	2.0 T
Magnet alignment accuracy	$< \pm 1$ mm
Injection pulses	12
Radius	1000 m
Energy gain rate	100–125 GeV/s
Cycling time (400 GeV)	12 s
Energy gain/turn	2.5 MeV
ν	19.4

[a] Fermi National Accelerator Laboratory.

securely to the tube. The assembly is supported in a vacuum cryostat by fiberglas supports, surrounded by a thermal shield at liquid nitrogen temperature. A flow of liquid helium maintains the low temperature of the magnet coils. Bending magnets in the energy doubler are 6.4 m in length. A total of 774 units are necessary. Quadrupoles are constructed in a similar manner; a total of 216 focusing magnets are required. The parameters of the FNAL accelerator are listed in Table 15.2.

Storage rings consist of bending and focusing magnets and a vacuum chamber in which high-energy particles can be stored for long periods of time. The background pressure must be very low to prevent particle loss through collisions. Storage rings are filled with particles by a high-energy synchrotron or a linear accelerator. Their geometry is almost identical to the separated function synchrotron. The main difference is that the particle energy remains constant. The magnetic field is constant, resulting in considerable simplification of the design. A storage ring may have one or more acceleration cavities to compensate for radiative energy loss of electrons or for longitudinal bunching of ions.

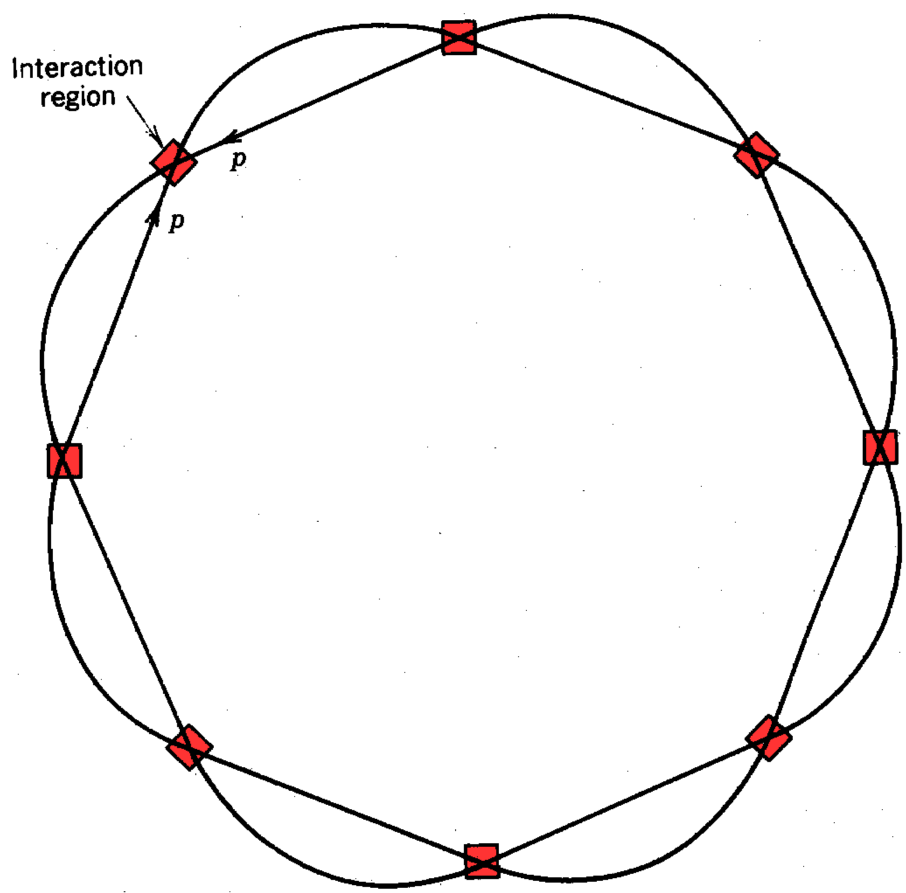

Figure 15.18 Arrangement of Intersecting Storage Ring, CERN.

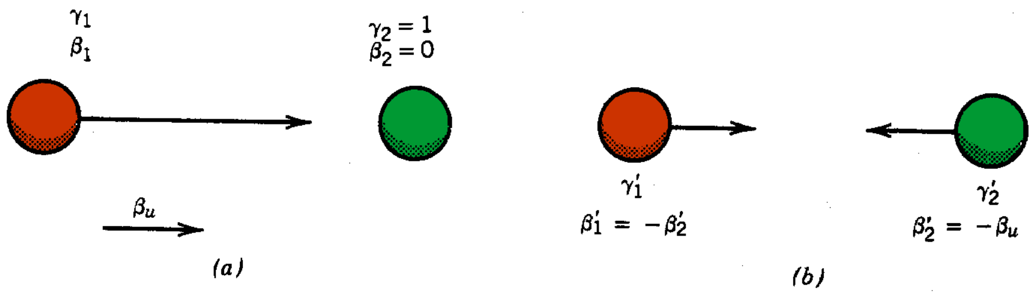

Figure 15.19 Collision of high-energy particle with target particle of equal rest mass. (*a*) View in stationary frame. (*b*) View in center-of-momentum frame.

One of the main applications of storage rings is in colliding beam facilities for high-energy particle physics. A geometry used in the ISR (intersecting storage ring) at CERN is shown in Figure 15.18. Two storage rings with straight and curved sections are interleaved. Proton beams circulating in opposite directions intersect at small angles at eight points of the ring. Proton-proton interactions are studied by detectors located near the intersection points.

Colliding beams have a significant advantage for high-energy physics research. The main requisite for probing the nature of elementary particles is that a large amount of energy must be available to drive reactions with a high threshold. When a moving beam strikes a stationary target (Fig. 15.19a), the kinetic energy of the incident particle is used inefficiently. Conservation of momentum dictates that a large portion of the energy is transformed to kinetic energy of the reaction products. The maximum energy available to drive a reaction in Figure 15.19a can be calculated by a transformation to the center-of-momentum (CM) frame. In the CM frame, the incident and target particles move toward one another with equal and opposite momenta. The reaction products need not have kinetic energy to conserve momentum when viewed in the CM frame; therefore, all the initial kinetic energy is available for the reaction.

For simplicity, assume that the rest mass of the incident particle is equal to that of the target particle. Assume the CM frame moves at a velocity $c\beta_u$ relative to the stationary frame. Using Eq. (2.30), the velocity of the target particle in the CM frame is given by

$$c\beta_2' = -c\beta_u, \tag{15.58}$$

and the transformed velocity of the incident particle is

$$c\beta_1' = c\ (\beta_1 - \beta_i)\ /\ (1 - \beta_u\beta_1). \tag{15.59}$$

Both particles have the same value of γ' in the CM frame; the condition of equal and opposite momenta implies

TABLE 15.3 Stationary Target: Available Reaction Energy (T_{cm}) Versus Incident Particle Kinetic Energy (T)

γ	γ'	T_{cm}/T $2(\gamma'-1)/(\gamma-1)$	T (protons) (GeV)	T_{cm} (protons) (GeV)
2.00	1.22	0.449	0.94	0.42
4.00	1.58	0.387	2.81	1.09
8.00	2.12	0.320	6.57	2.10
16.00	2.96	0.255	14.07	3.59
32.00	4.06	0.198	29.08	5.76
64.00	5.70	0.149	59.09	8.81
128.00	8.03	0.111	119.13	13.22
256.00	11.34	0.081	239.19	19.37
512.00	16.14	0.059	479.32	28.27
1024.00	23.41	0.044	959.57	42.22

$$-\beta_2' = \beta_1'. \tag{15.60}$$

Combining Eqs. (15.58), (15.59), and (15.60), we find that

$$\beta_u = (1/\beta_1) - \sqrt{(1/\beta_1^2) - 1}. \tag{15.61}$$

Equation (15.61) allows us to compare the energy invested in the incident particle,

$$T = (\gamma_1 - 1)\ m_o c^2, \tag{15.62}$$

to the maximum energy available for particle reactions,

$$T_{cm} = 2\ (\gamma_1' - 1)\ m_o c^2, \tag{15.63}$$

where

$$\gamma_1 = 1/\sqrt{1-\beta_1^2}, \qquad \gamma_1' = 1/\sqrt{1-\beta_u^2}.$$

Table 15.3 shows T_{cm}/T as a function of γ_1, along with equivalent kinetic energy values for protons. In the non-relativistic range, half the energy is available. The fraction drops off at high kinetic energy. Increasing the kinetic energy of particles striking a stationary target gives diminishing returns. The situation is much more favorable in an intersecting storage ring. The stationary frame is the CM frame. The CM energy available from ring particles with γ_1 is

$$T_{cm} = 2\ (\gamma_1 - 1)\ m_o c^2. \tag{15.63}$$

TABLE 15.4 High-Energy Accelerators and Storage Rings

Machine	Location	Particle	Energy
	Synchrotrons		
KEK	Tsukuba, Japan	p^+	12
ZGS (Zero-gradient synchrotron)	Argonne, Illinois, U.S.A.	p^+	12
CERN PS	Geneva, Switzerland	p^+	28
AGS (Alternating-gradient synchrotron)	Upton, New York, U.S.A.	p^+	32
Serpukhov	Serpukhov, USSR.	p^+	76
CERN SPS	Geneva, Switzerland	p^+	400
Fermilab	Batavia, Illinois, U.S.A.	p^+	800
Cornell Electron Synchrotron	Ithaca, New York, U.S.A.	e^-	12
DESY	Hamburg, Germany	e^-	7
	Linear Accelerator		
SLAC	Stanford, California, U.S.A.	e^-	25
	Colliding Beam Storage Rings		
ADONE	Frascati, Italy	e^-e^+	1.5 + 1.5
DCI	Orsay, France	e^-e^+	1.8 + 1.8
SLAC-SPEAR	Stanford, California, U.S.A.	e^-e^+	4 + 4
DESY-DORIS	Hamburg, Germany	e^-e^+	5 + 5
VEPP-4	Novosibirsk, USSR	e^-e^+	7 + 7
CESR	Ithaca, New York, U.S.A.	e^-e^+	8 + 8
SLAC-PEP	Stanford, California,	e^-e^+	18 + 18
DESY-PETRA	Hamburg, Germany	e^-e^+	19 + 19
CERN-ISR	Geneva, Switzerland	$p\bar{p}$	30 + 30

For example, a 21-GeV proton accelerator operated in conjunction with an intersecting storage ring can investigate the same reactions as a 1000-GeV accelerator with a stationary target. The price to pay for this advantage is reduction in the number of measurable events for physics experiments. A stationary target is usually at solid density. The density of a stored beam is more than 10 orders of magnitude lower. A major concern in intersecting storage rings is *luminosity*, a measure of beam density in physical space and velocity space. Given a velocity-dependent cross section, the luminosity determines the reaction rate between the beams. The required luminosity depends on the cross section of the reaction and the nature of the event detectors.

A list of accelerators and storage rings with the most energetic beams is given in Table 15.4. The energy figure is the kinetic energy measured in the accelerator frame. The history of accelerators for particle physics during the last 50 years has been one of an exponential increase in the available CM energy. Although this is attributable in part to an increase in the size of equipment, the main reason for the dramatic improvement has been the introduction of new acceleration techniques. When a particular technology reached the knee of its growth curve, a new type of accelerator was developed. For example, proton accelerators evolved from electrostatic machines to cyclotrons. The energy energy limit of cyclotrons was resolved by synchrocyclotrons which lead to the weak focusing synchrotron. The development of strong focusing made the construction of large synchrotrons possible. Subsequently, colliding beam techniques brought about a substantial increase in CM energy from existing machines. At present, there is considerable activity in converting the largest synchrotrons to colliding beam facilities.

In the continuing quest for high-energy proton beams for elementary particle research, the next stated goal is to reach a proton kinetic energy of 20 TeV (20×10^{12} eV). At present, the only identified technique to achieve such an extrapolation is to build an extremely large machine. A 20-TeV synchrotron with conventional magnets operating at an average field of I T has a radius of 66 km and a circumference of 414 km. The power requirements of conventional magnets in such a large machine are prohibitive; superconducting magnets are essential. Superconducting magnets can be designed in two ranges. Superconducting coils can be combined with a conventional pole assembly for fields below saturation. Because superconducting coils sustain a field with little power input, there is also the option for high-field magnets with completely saturated poles. A machine with 6-T magnets has a circumference of 70 km.

Studies have recently been carried out for a superconducting super collider (SSC) [see, M. Tigner, Ed., *Accelerator Physics Issues for a Superconducting Super Collider,* University of Michigan, UM HE 84-1, 1984]. This machine is envisioned as two interleaved 20-TeV proton synchrotrons with counter-rotating beams and a number of beam intersection regions. Estimates of the circumference of the machine range from 90 to 160 km, depending on details of the magnet design. The CM energy is a factor of 40 higher than that attainable in existing accelerators. If it is constructed, the SSC may mark the termination point of accelerator technology in terms of particle energy; it is difficult to imagine a larger machine. Considerations of cost versus rewards in building the SSC raise interesting questions about economic limits to our knowledge of the universe.

15.6 LONGITUDINAL DYNAMICS OF SYNCHROTRONS

The description of longitudinal particle motion in synchrotrons has two unique aspects compared to synchrocyclotrons and AVF cyclotrons. The features arise from the geometry of the machine and the high energy of the particles:

1. Variations of longitudinal energy associated with stable phase confinement of particles in an rf bucket result in horizontal particle oscillations. The synchrotron oscillations sum with the usual betatron oscillations that arise from spreads in transverse velocity. Synchrotron oscillations must be taken into account in choosing the size of the *good field* region of focusing magnets.

2. The range of stable synchronous phase in a synchrotron depends on the energy of particles. This effect is easily understood. At energies comparable to or less than $m_o c^2$, particles are non-relativistic; therefore, their velocity depends on energy. In this regime, low-energy particles in a beam bunch take a longer time to complete a circuit of the accelerator and return to the acceleration cavity. Therefore, the accelerating voltage must rise with time at φ_s for phase stability ($0 < \varphi_s < \pi/2$). At relativistic energies, particle velocity is almost independent of energy; the particle orbit circumference is the main determinant of the revolution time. Low-energy particles have smaller orbit radii and therefore take less time to return to the acceleration gap. In this case, the range of stable phase is $\pi/2 < \varphi_s < \pi$. The energy that divides the regimes is called the *transition energy*. In synchrotrons that bridge the transition energy, it is essential to shift the phase of the rf field before the bunched structure of the beam is lost. This effect is unimportant in electron synchrotrons because electrons are always injected above the transition energy.

Models are developed in this section to describe the longitudinal dynamics of particles in synchrotrons. We begin by introducing the quantity γ_t, the transition gamma factor. The parameter characterizes the dependence of particle orbit radius in the focusing lattice to changes in momentum. We shall see that γ_t corresponds to the relativistic mass factor at the transition energy. After calculating examples of γ_t in different focusing systems, we shall investigate the equilibrium conditions that define a synchronous phase. The final step is to calculate longitudinal oscillations about the synchronous particle.

The transition gamma factor is defined by

$$\gamma_t^2 = \frac{\delta p/p_s}{\delta S/S}, \tag{15.64}$$

where p_s is the momentum of the synchronous particle and S is the pathlength of its orbit around the machine. In a circular accelerator with no straight sections, the equilibrium radius is related to pathlength by $S = 2\pi R$; therefore,

$$\gamma_t^2 = \frac{\delta p/p_s}{\delta R/R}, \tag{15.65}$$

The transition gamma factor must be evaluated numerically for noncircular machines with complex lattices. We will develop simple analytic expressions for γ_t in ideal circular accelerators with weak and strong focusing.

In a weak focusing synchrotron, momentum is related to vertical magnetic field and position by Eq. (3.38), $p = qrB$, so that

$$\delta p/p_s = (\delta r/R) + (\delta B/B_o). \tag{15.66}$$

for $\delta r \ll R$ and $\delta B \ll B_o$. The relative change in vertical field can be related to the change in radius though Eq. (7.18), so that

$$\gamma_t^2 = \frac{\delta p/p_s}{\delta r/R} = (1 - n) = \left(\frac{\omega_r}{\omega_{go}}\right)^2. \tag{15.67}$$

The requirement of stable betatron oscillations in a weak focusing machine limits γ_t to the range $0 < \gamma_t < 1$.

We can also evaluate γ_t for an ideal circular machine with uniform bending field and a strong focusing system. Focusing in the radial direction is characterized by ν_r, the number of radial betatron oscillations per revolution. For simplicity, assume that the particles are relativistic so that the magnetic forces are almost independent of energy. The quantity R is the equilibrium radius for particles of momentum $\gamma_o m_o c$. The radial force expanded about R is

$$F_r \cong -\gamma_o m_o \omega_r^2 \, \delta r - qB_o c, \tag{15.68}$$

where $\delta r = r - R$. The equilibrium radius for momentum $(\gamma_o + \delta\gamma)\, m_o c$ is determined by the balance of magnetic forces with centrifugal force, $(\gamma_o + \delta\gamma)\, m_o c^2/r$. Neglecting second-order terms, we find that

$$\gamma_o m_o \omega_r^2 \, \delta r + qB_o c \cong \gamma_o m_o c^2/R + \delta\gamma m_o c^2/R - \gamma m_o c^2 \, \delta r/R^2. \tag{15.69}$$

Zero-order terms cancel, leaving

$$(\delta r/R)\ (\omega_r^2 + \omega_{go}^2) \cong (\delta\gamma/\gamma_o)\ \omega_{go}^2 \cong (\delta p/p)\ \omega_{go}^2,$$

or

$$\gamma_t^2 \cong 1 + (\omega_r/\omega_{go})^2 = 1 + \nu_r^2. \tag{15.70}$$

Note that $\gamma_t \gg 1$ in a strong focusing system with high ν_r. Therefore, particle position in a strong focusing system is much less sensitive to momentum errors than in a weak focusing system.

Both the magnetic field and frequency of accelerating electric fields must vary in a synchrotron to maintain a synchronous particle with constant radius *R*. There are a variety of possible acceleration histories corresponding to different combinations of synchronous phase, cavity voltage amplitude, magnetic field strength, and rf frequency. We shall derive equations to relate the different quantities.

We begin by calculating the momentum of the synchronous particle as a function of time. Assume the acceleration gap has narrow width δ so that transit-time effects can be neglected. The electric force acting on the synchronous particle in a gap with peak voltage V_o is

$$qE = (qV_o\ \sin\varphi_s/\delta). \tag{15.71}$$

The momentum change passing through the gap is the electric force times the transit time, or

$$\Delta p_s = (qV_o\ \sin\varphi_s/\delta)\ (\delta/v_s), \tag{15.72}$$

where v_s is the synchronous particle velocity. Acceleration occurs over a large number of revolutions; it is sufficient to approximate p_s as a continuous function of time. The smoothed derivative of p_s is found by dividing both sides of Eq. (15.72) by the revolution time

$$\tau_o = 2\pi R/v_s. \tag{15.73}$$

The result is

$$dp_s/dt \cong qV_o\ \sin\varphi_s/2\pi R. \tag{15.74}$$

If V_o and φ_s are constant, Eq. (15.74) has the solution

$$p_s = p_{so} + (qV_o\ \sin\varphi_s/2\pi R)\ t. \tag{15.75}$$

Either Eq. (15.74) or (15.75) can be used to find $p_s(t)$. Equation (2.37) can then be used to determine γ_s(t) from $p_s(t)$. The time history of the frequency is then constrained. The revolution frequency is $\omega_{go} = v_s/R = (c/R)\sqrt{1 - 1/\gamma_s^2}$ through Eq. (2.21). The rf frequency must be an integer multiple of the revolution frequency, $\omega = M\omega_{go}$. In small synchrotrons, M may equal 1 to minimize the rf frequency. In larger machines, M is usually greater than unity. In this case, there are M circulating beam bunches contained in the ring. The rf frequency is related to the particle energy by

$$\omega = (Mc/R)\sqrt{1 - 1/\gamma_s^2}. \tag{15.77}$$

Similarly, the equation $B_o = \gamma_o m_o v_s/qR$ implies that the magnetic field magnitude is

$$B_o = (m_o c/qR)\sqrt{\gamma_s^2 - 1}. \tag{15.78}$$

The rf frequency and magnetic field are related to each other by

$$\omega = \frac{MqB_o/m_o}{\sqrt{1 + (qB_oR/m_oc)^2}}\ . \tag{15.79}$$

As an example of the application of Eqs. (15.75), (15.77), and (15.78), consider the parameters of a moderate-energy synchrotron (the Bevatron). The injection and final energies for protons are 9.8 MeV and 6.4 GeV. The machine radius is 18.2 m and $M = 1$. The variations of rf frequency and B_o during an acceleration cycle are plotted in Figure 15.20. The magnetic field rises from 0.025 to 1.34 T and the frequency ($f = \omega/2\pi$) increases from 0.37 to 2.6 MHz.

The reasoning that leads to Eq. (15.74) can also be applied to derive a momentum equation for a nonsynchronous particle. Again, averaging the momentum change around one revolution,

$$dp/dt \cong (qV_o/2\pi R)\ \sin\varphi, \tag{15.80}$$

where R is the average radial position of the particle. Substituting $\delta p = p - p_s$, we find (as in Section 13.3) that

$$d\delta p/dt = (qV_o/2\pi R)\ (\sin\varphi - \sin\varphi_s) = (qV_o\omega_{go}/2\beta_s c)\ (\sin\varphi - \sin\varphi_s). \tag{15.81}$$

Applying Eq. (15.6), changes of phase can be related to the difference between the orbital frequency of a nonsynchronous particle to the rf frequency,

$$d\varphi/dt = \omega - M\omega_g. \tag{15.82}$$

The orbital frequency must be related to variations of relativistic momentum in order to generate a closed set of equations. The revolution time for a nonsynchronous particle is $\tau = 2\pi r/v = 2\pi/\omega_g$,

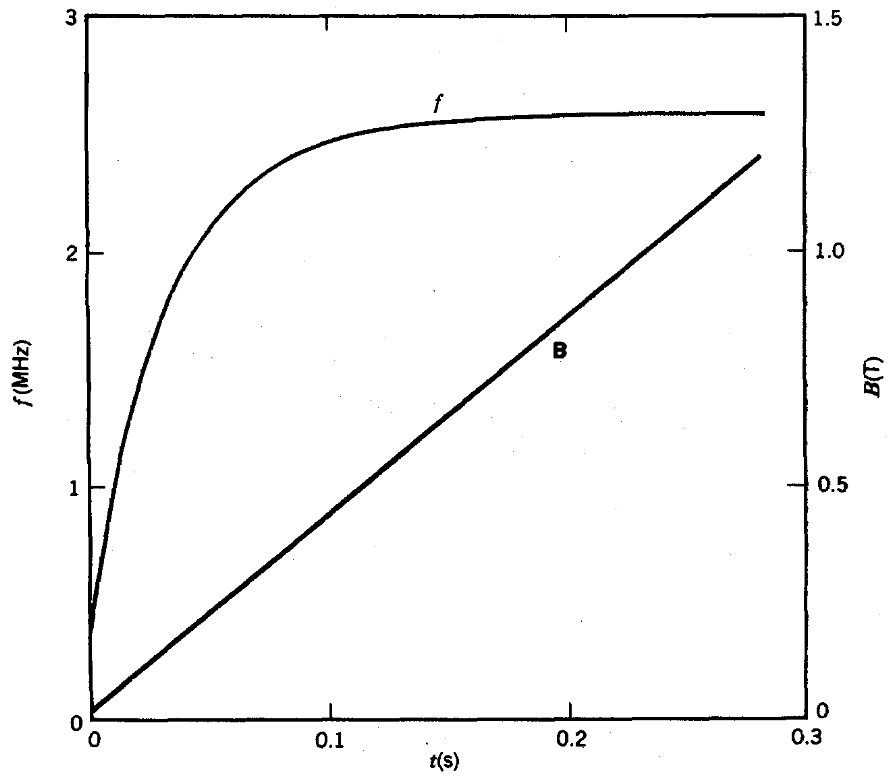

Figure 15.20 Variation of magnetic field and rf frequency during acceleration cycle of protons from 9.4 MeV to 5.6 GeV (Bevatron).

Differential changes in τ arise from variations in particle velocity and changes in orbit radius. The following equations pertain to small changes about the parameters of the synchronous particle orbit:

$$\delta\tau/\tau_o = -\delta\omega_g/\omega_{go} = (\delta r/R) - (\delta v/v_s) = (\delta r/R) - (\delta\beta/\beta_s). \tag{15.83}$$

The differential change in momentum ($p = \gamma m_o \beta c$) is

$$(\delta p/p_s) = \delta\gamma/\gamma_o + \delta\beta/\beta_s = \delta\beta/\beta_s \;/\; (1 - \beta_s^2). \tag{15.84}$$

The final form is derived from Eq. (2.22) with some algebraic manipulation. Noting that $\delta\beta/\beta_s = (1 - \beta_s^2)\,(\delta p/p_s)$, we find that

$$-\delta\omega_g/\omega_{go} = (\delta r/R) - (\delta p/p_s) \;/\; \gamma_s^2 = [(1/\gamma_t^2) - (1/\gamma_s^2)]\,(\delta p/p_s). \tag{15.85}$$

Equation (15.85) implies that

$$d\omega_g/dt = -(d\delta p/dt)\ (\omega_{go}/p_s)\ [(1/\gamma_t^2) - (1/\gamma_s^2)]. \tag{15.86}$$

Equations (15.81), (15.82), and (15.86) can be combined into a single equation for phase in the limit that the parameters of the synchronous particle and the rf frequency change slowly compared to the time scale of a phase oscillation. This is an excellent approximation for the long acceleration cycle of synchrotrons. Treating ω as a constant in Eq. (15.82), we find

$$d^2\varphi/dt^2 = -M\ (d\omega_g/dt). \tag{15.87}$$

Combining Eqs. (15.85), (15.86), and (15.87), the following equation describes phase dynamics in the synchrotron:

$$d^2\varphi/dt^2 = (M\omega_{go}^2/\gamma_o m_o c^2\beta_s^2)\ (eV_o/2\pi)\ [(1/\gamma_t^2) - (1/\gamma_s^2)]\ (\sin\varphi - \sin\varphi_s). \tag{15.88}$$

Equation (15.88) describes a nonlinear oscillator; it is similar to Eq. (13.21) with the exception of the factor multiplying the sine functions. We discussed the implications of Eq. (13.21) in Section 13.3, including phase oscillations, regions of acceptance for longitudinal stability, and compression of phase oscillations. Phase oscillations in synchrotrons have two features that are not encountered in linear accelerators:

1. Phase oscillations lead to changes of momentum about p_s and hence to oscillation of particle orbit radii. These radial oscillations are called *synchrotron oscillations*.

2. The coefficient of the sine terms may be either positive or negative, depending on the average particle energy.

In the limit of small phase excursion ($\Delta\varphi \ll 1$), the angular frequency for phase oscillations in a synchrotron is

$$\omega_s = \omega_{go} \sqrt{-\frac{M\cos\varphi_s}{2\pi\beta_s^2}\ \frac{eV_o}{\gamma_s m_o c^2} \left(\frac{1}{\gamma_t^2} - \frac{1}{\gamma_s^2} \right)} \tag{15.89}$$

Note that the term in brackets contains dimensionless quantities and a factor proportional to the ratio of the peak energy gain in the acceleration gap divided by the particle energy. This is a very small quantity; therefore, the synchrotron oscillation frequency is small compared to the frequency for particle revolutions or betatron oscillations. The radial oscillations occur at angular frequency

w_s. In the range well beyond transition ($\gamma_s \gg \gamma_t$), the amplitude of radial oscillations can be expressed simply as

$$\delta r \cong R\ (\Delta\varphi/M)\ (\omega_s/\omega_{go}), \tag{15.90}$$

where $\Delta\varphi$ is the maximum phase excursion of the particle from φ_s.

The behavior of the expression $[(1/\gamma_t^2) - (1/\gamma_s^2)]$ determines the range of stable phase and the transition energy. For large γ_t or small γ_s, the expression is negative. In this case, the stability range is the same as in a linear accelerator, $0 < \varphi_s < \pi/2$. At high values of γ_s, the sign of the expression is positive, and the stable phase regime becomes $\pi/2 < \varphi_s < \pi$.

In a weak focusing synchrotron, γ_t is always less than unity; therefore, particles are in the post-transition regime at all values of energy. Transition is a problem specific to strong focusing synchrotrons. The transition energy in a strong focusing machine is given approximately by

$$E_t = (m_o c^2)\ \nu_r. \tag{15.91}$$

15.7 STRONG FOCUSING

The strong focusing principle [N. C. Christofilos, U.S. Patent No. 2,736,799 (1950)] was in large part responsible for the development of synchrotrons with output beam kinetic energy exceeding 10 GeV. Strong focusing leads to a reduction in the dimensions of a beam for a given transverse velocity spread and magnetic field strength. In turn, the magnet gap and transverse extent of the *good field region* can be reduced, bringing about significant reductions in the overall size and cost of accelerator magnets.

Weak focusing refers to beam confinement systems in circular accelerators where the betatron wavelength is longer than the machine circumference. The category includes the gradient-type field of betatrons and uniform-field cyclotrons. Strong focusing accelerators have $\lambda_b < 2\pi R$, a consequence of the increased focusing forces. Examples are the alternating-gradient configuration and *FD* or *FODO* combinations of quadrupole lenses. Progress in rf linear accelerators took place largely in the early 1950s after the development of high-power rf equipment. Although some early ion linacs were built with solenoidal lenses, all modem machines use strong focusing quadrupoles, either magnetic or electric.

The advantage of strong focusing can be demonstrated by comparing the vertical acceptance of a weak focusing circular accelerator to that of an altemating-gradient (AG) machine. Assume that the AG field consists of *FD* focusing cells of length I (along the beam orbit) with field index $\pm n$, where $n \gg 1$. The vertical position of a particle at cell boundaries is given by

$$z = z_o\ \cos(M\mu + \varphi), \tag{15.92}$$

where

$$\mu = \cos^{-1} [\cos(\sqrt{n}\omega_{go}/v_s)\ \cosh(\sqrt{n}\omega_{go}/v_s)]$$

and M is the cell number. For $\mu \leq 1$, the orbit consists of a sinusoidal oscillation extending over many cells with small-scale oscillations in individual magnets. Neglecting the small oscillations, the orbit equation for particles on the beam envelope is

$$z \cong z_o \cos(\mu S/l + \varphi), \tag{15.93}$$

where S, the distance along the orbit, is given by $S = Ml$. The angle of the orbit is approximately

$$z' \cong -(z_o\mu/l)\ \sin(\mu S/l + \varphi). \tag{15.94}$$

Combining Eqs. (15.93) and (15.94), the vertical acceptance is

$$A_v = \pi z_o z_o' = \pi z_o^2 \mu/l. \tag{15.95}$$

In a weak focusing system, vertical orbits are described by

$$z \cong z_o \cos(\sqrt{n}S/R + \varphi). \tag{15.96}$$

Following the same development, the vertical acceptance is

$$A_v = \pi z_o^2 \sqrt{n}/R. \tag{15.97}$$

In comparing Eqs. (15.95) and (15.97), note that the field index for weak focusing must be less than unity. In contrast, the individual field indices of magnets in the alternating gradient are made as large as possible, consistent with practical magnet design. Typically, the field indices are chosen to give $\mu \sim 1$. For the same field strength, the acceptance of the strong focusing system is therefore larger by a factor on the order of R/l or $N/2\pi$, where N is the number of focusing cells. The quantity N is a large number. For example, $N = 60$ in the AGS accelerator at Brookhaven National Laboratory.

The major problem of strong focusing systems is that they are sensitive to alignment errors and other perturbations. The magnets of a strong focusing system must be located precisely. We shall estimate the effects of alignment error in a strong focusing system using the transport matrix formalism (Chapter 8). The derivation gives further insight into the origin of resonant instabilities introduced in Section 7.2.

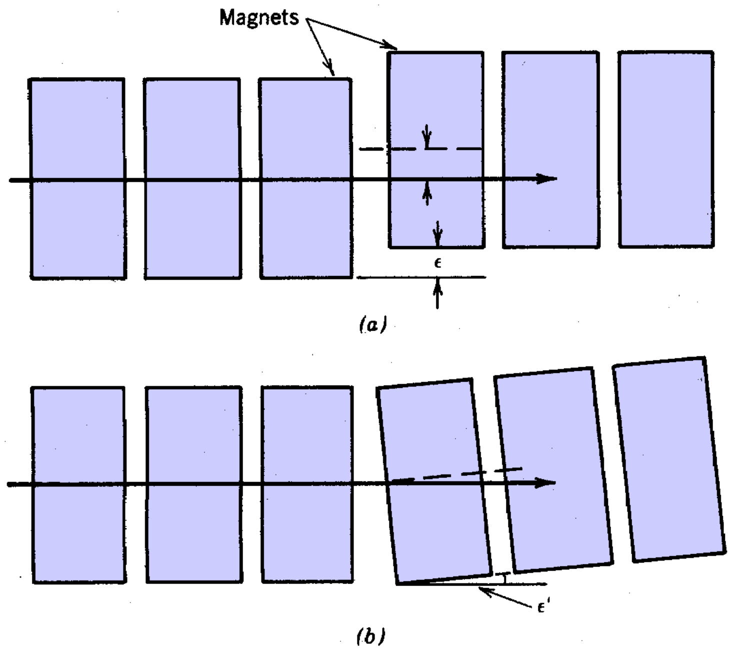

Figure 15.21 Alignment errors between magnets in strong focusing system. (*a*) Error in position. (*b*) Error in angle.

For simplicity, consider a circular strong focusing machine with uniformly distributed cells. Assume that there is an error of alignment in either the horizontal or vertical direction between two cells. The magnets may be displaced a distance ε, as shown in Figure 15.21a. In this case, the position component of an orbit vector is transformed according to

$$x \Rightarrow x + \varepsilon \qquad (15.98)$$

when the particle crosses the boundary. An error in magnet orientation by an angle ε' (Fig. 15.21b) causes a change in the angular part of the orbit vector:

$$x' \Rightarrow x' + \varepsilon' \qquad (15.99)$$

The general transformation at the boundary is

$$\boldsymbol{u}_{n+1} = \boldsymbol{u}_n + \boldsymbol{\varepsilon}, \qquad (15.100)$$

where $\boldsymbol{\varepsilon} = (\varepsilon, \varepsilon')$.

Let $\boldsymbol{A}$ be the transfer matrix for a unit cell of the focusing system and assume that there are N cells distributed about the circle. The initial orbit vector of a particle is $\mathbf{u}_0$. For convenience, $\mathbf{u}_0$ is defined at a point immediately following the imperfection. After a revolution around the machine and traversal of the field error, the orbit vector becomes

$$\boldsymbol{u}_N = \boldsymbol{A}^N \boldsymbol{u}_0 + \boldsymbol{\varepsilon}. \tag{15.101}$$

The orbit vector after two revolutions, is

$$\boldsymbol{u}_{2N} = \boldsymbol{A}^N \boldsymbol{u}_N + \boldsymbol{\varepsilon} = \boldsymbol{A}^{2N} \boldsymbol{u}_0 + (\boldsymbol{A}^N + \boldsymbol{I})\ \boldsymbol{\varepsilon}, \tag{15.102}$$

where $\boldsymbol{I}$ is the identity matrix. By induction, the transformation of the orbit matrix for n resolutions is

$$\boldsymbol{u}_{nN} = \boldsymbol{A}^{nN} \boldsymbol{u}_0 + \boldsymbol{D}_n\boldsymbol{\varepsilon}. \tag{15.103}$$

where

$$\boldsymbol{D}_n = (\boldsymbol{A}^{(n-1)N} + \boldsymbol{A}^{(n-2)N} + \ldots + \boldsymbol{A}^N + \boldsymbol{I}). \tag{15.104}$$

We found in Chapter 8 that the first term on the right-hand side of Eq. 1(15.103) corresponds to bounded betatron oscillations when stability criteria are satisfied. The amplitude of the term is independent of the perturbation. Particle motion induced by the alignment error is described by the second term. The expression for $\boldsymbol{D}_{\mathrm{n}}$ can be simplified using the eigenvectors (Section 8.6) of the matrix $\boldsymbol{A}$: $\mathbf{v}_1$ and $\mathbf{v}_2$. The eigenvectors form a complete set; any two-dimensional vector, including $\boldsymbol{\varepsilon}$ can be resolved into a sum of eigenvectors:

$$\boldsymbol{\varepsilon} = a_1\ \mathbf{v}_1 + a_2\ \mathbf{v}_2. \tag{15.105}$$

We found in Section 8.6 that the eigenvalues for a transfer matrix $\boldsymbol{A}$ are

$$\lambda_1 = \exp(\ j\mu), \qquad \lambda_2 = \exp(-j\mu). \tag{15.106}$$

where μ is the phase:advance in a cell. Substituting Eq. (15.106) in Eq. (15.103), we find

$$\begin{aligned} \boldsymbol{D}_n\boldsymbol{\varepsilon} &= a_1\ \nu_1 \left[\ \exp[j(n-1)N\mu] + \exp[j(n-2)N\mu] + \ldots + 1\ \right] \\ &+ a_2\ \nu_2 \left[\ \exp[-j(n-1)N\mu] + \exp[-j(n-2)N\mu] + \ldots + 1\ \right], \end{aligned} \tag{15.107}$$

The sums of the geometric series can be rewritten as

$$\boldsymbol{D}_n\varepsilon = \frac{\exp(jnN\mu) - 1}{\exp(jN\mu) - 1} a_1 \nu_1 + a\frac{\exp(-jnN\mu) - 1}{\exp(-jN\mu) - 1} a_2 \nu_2. \tag{15.108}$$

or, alternately,

$$\boldsymbol{D}_n\varepsilon = [\sin(nN\mu/2)/\sin(n\mu/2)]$$
$$\times [\exp[j(n-1)N\mu/2)] a_1 \nu_1 + \exp[-j(n-1)N\mu/2)] a_2 \nu_2]. \tag{15.109}$$

The second term in braces is always bounded; it has a magnitude on the order of ε. The first term in brackets determines the cumulative effect of many transitions across the alignment error. The term becomes large when the denominator approaches zero; this condition occurs when

$$\mu = 2\pi M/N, \tag{15.110}$$

where M is an integer. Equation (15.110) can be rewritten in terms of ν, the number of betatron wavelengths per revolution:

$$\nu = M. \tag{15.111}$$

This is the condition for an orbital resonance. When there is a resonance, the effects of an alignment error sum on successive revolutions. The amplitude of oscillatory motion grows with time. The motion induced by an error when $\nu \neq M$ is an oscillation superimposed on betatron and synchrotron oscillations. The amplitude of the motion can be easily estimated. For instance, in the case of a position error of magnitude ε, it is $\varepsilon/\sin(N\mu/2)$.

TABLE 15.5 Forbidden ν Values[a]

Condition	Description
$\nu_r, \nu_z = M$	Magnet misalignment, error in field strength
$\nu_r, \nu_z = M/2$	Error in field index of bending magnets.
$\nu_r, \nu_z = N$ or $N/2$	Particularly strong special case of conditions 1 or 2, where N is the number of focusing cells in the circular machine.
$\nu_r, \nu_z = N'$ or $N'/2$	Another special case of 1 or 2, where N' is the number of superperiods in a machine with curved and straight sections.
$\nu_r + \nu_z = M$	Linear coupling between horizontal and vertical betatron oscillations. Induced by rotational error in a quadrupole focusing magnet.

[a] M, N, and N' are integers.

An alternate view of the nature of resonant instabilities, mode coupling, is useful for general treatments of particle instabilities. The viewpoint arises from conservation of energy and the second law of thermodynamics. The second law implies that there is equipartition of energy between the various modes of oscillation of a physical system in equilibrium. In the treatment of resonant instabilities in circular accelerators, we included two modes of oscillation: (1) the revolution of particles at frequency ω_{go} and (2) betatron oscillations. There is considerable longitudinal energy associated with particle revolution and, under normal circumstances, a small amount of energy in betatron oscillations.

In a linear analysis, there is no exchange of energy between the two modes. A field error introduces a nonlinear coupling term, represented by $\boldsymbol{D_n \varepsilon}$ in Eq. (15.103). This term allows energy exchange. The coupling is strong when the two modes are in resonance. The second law implies that the energy of the betatron oscillations increases. A complete nonlinear analysis predicts that the system ultimately approaches an equilibrium with a thermalized distribution of particle energy in the transverse and longitudinal directions. In an accelerator, the beam is lost on vacuum chamber walls well before this state is reached.

In a large circular accelerator, there are many elements of periodicity that can induce resonance coupling of energy to betatron oscillations. In synchrotrons, where particles are contained for long periods of time, all resonance conditions must be avoided. Resonances are categorized in terms of forbidden numbers of betatron wavelengths per revolution. The physical bases of some forbidden values are listed in Table 15.5.